12-2013

Inkjet Printing of Titanium Dioxide Photoanodes for Dye Sensitized Solar Cells

Jeffrey Corbet Johnson
Grand Valley State University

Inkjet printing of titanium dioxide photoanodes for dye sensitized solar cells

Jeffrey Corbet Johnson

A Thesis Submitted to the Graduate Faculty of

GRAND VALLEY STATE UNIVERSITY

In

Partial Fulfillment of the Requirements

For the Degree of

Masters of Science

Electrical Engineering

December 2013

Acknowledgements

The author would like to express his sincere appreciation to Dr. Heidi Jiao for invaluable guidance and support through the duration of the research project. Additionally, the feedback contributed by the advisory committee, Dr. Bruce Dunne and Dr. Nael Barakat, was especially helpful in improving the finished work.

This project was supported by Grand Valley State University's School of Engineering through the provision of laboratory access and supplies. In particular, the assistance of Ron Grew is gratefully acknowledged.

Abstract

Dye Sensitized Solar Cells (DSSC) offer advantages over semiconductor solar cells including lower costs and relaxed material purity requirements. However, DSSC solar energy conversion efficiencies are lower than many competing photovoltaic technologies. Key to DSSC performance is the incorporation of nanocrystalline metal oxides to provide a large surface area for photosensitive dye loading. Titanium dioxide (TiO_2) is the predominately used metal oxide. The structure of the TiO_2 layer determines charge transfer efficiency and the level of generated photocurrent. Common practice for high performance cells is to deposit a thin, compact TiO_2 coating followed by a thicker, more porous TiO_2 layer. Often, different deposition methods are used for each layer.

Inkjet printing of TiO_2 potentially offers a high degree of control over the deposition of TiO_2 suspensions. Previous use of inkjet printing for TiO_2 depositions have focused on producing TiO_2 films with uniform density. A multi-ink printing system offers the possibility of forming TiO_2 films with variable density using a single deposition method.

For this research, inkjet printing of TiO_2 films with a graded density profile was explored as a means of improving DSSC performance. Cell performance was assessed through the measurement of generated currents and device Fill Factors.

Two means to produce density variations in TiO_2 layers were explored: TiO_2 particle size and layer pore-volume. For the former, the reduction of micron-sized TiO_2 particles using a milling approach was attempted but proved unsuccessful. To affect changes in pore-volume, several TiO_2 suspensions were developed with varying pore-forming content that successfully produced variations in layer density. DSSCs with printed TiO_2 films having three density layers showed an average improvement in the Fill Factor of 8% versus single layers and 6% versus

double layers. Short-circuit currents in tri-layer films increased an average of 35% over single layers and 13% over double layers.

The results effectively demonstrated the potential for using inkjet printing as a sole deposition method to produce TiO_2 films with a non-uniform density leading to improved DSSC performance. One possibility for further study would be to create further layer variations through the simultaneous printing of different suspensions.

Keywords: Dye sensitized solar cells, TiO_2 deposition, inkjet printing, photovoltaics

Table of Contents

List of Acronyms and Abbreviations

Atomic force microscope	AFM
Dye sensitized solar cell	DSSC
Energy relay dye	ERD
Fluorine tin oxide	FTO
Highest occupied molecular orbital	HOMO
Hole-transport material	HTM
Indium tin oxide	ITO
Iodide	I
Lowest unoccupied molecular orbital	LUMO
Platinum	Pt
Polyethylene glycol	PEG
Quantum dot sensitized solar cells	QDSSC
Ruthenium	Ru
Scanning electron microscope	SEM
Silicon dioxide	SiO_2
Titanium dioxide	TiO_2
Transparent Conducting Oxide	TCO

1 Introduction

A major attraction of Dye sensitized solar cells (DSSC), a type of electrochemical solar cell, is the relative simplicity of their fabrication. Unlike multi-junction semiconductor solar cells that require complicated and expensive fabrication processes or crystalline silicon cells that require high material purities, DSSCs can be produced using simpler procedures and relatively lax purity standards. Modern DSSCs have benefited from significant material advances over the original electrochemical solar cells. In particular, the incorporation of nano-structured semiconductors into DSSC designs revolutionized the performance and prospects of electrochemical cells. Appendix A provides an overview of other photovoltaic technologies.

1.1 DSSC Overview

Electrochemical cells have a relatively simple structure. One side of the cell is the photo-electrode made up of a Transparent conduction oxide (TCO) substrate coated with a semiconductor layer; the other side is the counter electrode which consists of a catalyzing material deposited on a second TCO substrate. The two halves are bonded together face-to-face and an electrolyte is injected into the space between them. When the semiconductor layer is coated with a photo-sensitive dye, the cell is a DSSC.

1.1.1 DSSC Components

There are well established materials that comprise a "standard" DSSC: Titanium dioxide (TiO_2) semiconducting nanoparticles, Ruthenium-based (Ru) dyes, Iodide-based (I^-/I_3^-) electrolytes, a Platinum (Pt) catalyst, and Transparent Conducting Oxides (TCOs) as a substrate. Fluorine doped tin oxide (FTO) is a commonly selected TCO. Indium tin oxide (ITO) has also seen wide usage.

Figure 1 shows the major elements and their arrangement in a standard DSSC.

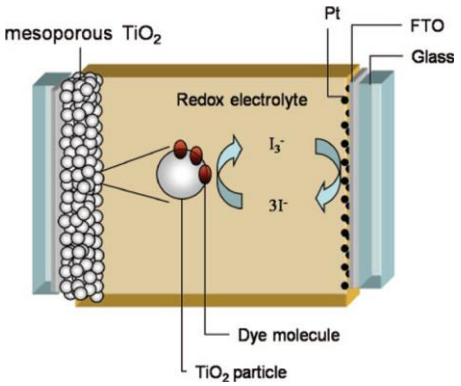

Figure 1: Common materials in a DSSC and their structural configuration in a standard DSSC [1].

Investigations into material variations have often involved attempts to reduce material costs or to simplify processing procedures rather than to necessarily improve overall device performance. Optimization of material and processing costs represents an important step in enhancing the commercial viability of DSSCs. A sampling of different research avenues being pursued in the area of material selection, overall cost, and device performance is offered in Appendix B.

1.1.2 DSSC Operating Principles

As the macroscopic electric field in electrochemical cells is screened by the ions in the electrolyte, the charge transport through the cell occurs in a fundamentally different way than in traditional single junction solar cells [2]. The electrolyte present between the photoactive semiconductor electrode and the catalyzing counter electrode facilitates a change from an electronic transport mode to an ionic one.

Electron/hole pairs are produced when photons of sufficient energy oxidize a dye molecule and charge separation occurs when the photoelectron is injected into the semiconductor; the electrons are collected at the back surface of the semiconductor and the holes accumulate at the semiconductor/electrolyte interface [3]. The voltage produced by the cell

results from the difference between the semiconductor's Fermi level and the electrolyte redox potential [1].

1.1.3 Development of DSSCs

Originally, electro-chemical PV cells used traditional semiconductors such as silicon but suffered from photocorrosion of the semiconductors when illuminated while immersed in the liquid electrolytes. Semiconductors such as Titanium dioxide (TiO_2) were selected as a chemically-stable replacement but possessed significantly lower spectral responses. TiO_2 absorbs light in the UV region but is transparent to visible light [4].

One means of solving this issue was to introduce sensitizing dyes into the electrochemical cells. The incorporation of photo-sensitive dyes on the surface of the semiconductor allowed for tuning of the spectral response of the cell. Electron/hole pairs were then generated within the dye as dye molecules became oxidized by incident light; electrons moved into the semiconductor and holes moved to the dye/electrolyte interface. Re-oxidation of dye molecules occurred by the ionic charge transport action of the electrolyte.

The major innovation to the electrochemical cell was the use of nano-structured metal oxide semiconductors at the photo-electrode by Gratzel and his colleagues. The nano-structuring of the semiconductor produced a dramatic increase in the surface area available for dye attachment.

The most widely used metal oxide, and the one used by Gratzel, is TiO_2. Electrochemical cells with dye-sensitized, nanostructured semiconductor photo-electrodes are sometimes referred to as Gratzel cells. State of the art DSSCs have reached efficiencies of 15% [5]. Compared to crystalline silicon solar cells with efficiencies approaching theoretical maximums, the efficiencies of DSSC cells have yet to realize their full potential.

1.2 TiO_2 Layers in Dye Sensitized Solar Cells

State of the art DSSCs have used a layered TiO_2 architecture [6]. Directly on the surface of a TCO substrate, a dense, a 50nm layer of TiO_2 is deposited to protect the FTO from the electrolyte solution. The main light absorption layer is applied to the top of the base layer and is typically 10 microns thick. The target particle size for this layer is 20nm. Poly ethylene glycol (PEG), a pore-forming agent, is often added to increase the porosity to ensure a large surface area for dye loading. For the DSSC with the highest reported performance, the initial, compact layer was deposited by spray coating and the second layer by spin-coating [5].

Reducing the process of forming TiO_2 films to a single deposition step are desirable to simplify the DSSC fabrication. Single layer TiO_2 depositions can show a substantial decrease in cell energy conversion efficiency to less than 3% compared to the 15% obtained by state of the art cells [5, 7]. For the best performance, the TiO_2 film formation process benefits need to provide the film with properties that provide the necessary surface area while maintaining good conductivity.

1.2.1 TiO_2 Particle Size and Layer Pore Volume

Two properties of the TiO_2 layer are vitally important to the performance of a standard DSSC: the TiO_2 particle size and the porosity of the surface. Ideally, the TiO_2 particle size is as consistently small as possible throughout a deposited layer. A highly porous surface allows for an increased surface area for dye attachment and electrolyte penetration. The layer must also have good electrical contact with the underlying substrate to minimize series resistance.

Efficient transport of photoelectrons through a nano-crystalline semiconductor is heavily reliant on the conductive connectivity of individual particles as well as with the conductive path through the layer and to the substrate. A dense TiO_2 film would enhance both of these

characteristics but would reduce the surface area of the layer decreasing the amount of dye that could be loaded. A reduction in particle connectivity with a more porous layer would result in the layer having reduced charge transport capacity through the film. A poorly conductive interface between the semiconductor and the substrate would result in a higher series resistance and lower photocurrents.

These properties are largely dependent on two factors: the preparation process used to generate a TiO_2 nanoparticle suspension and the deposition technique.

X-ray diffraction (XRD) is a standard method for determining crystallite sizes present in a nano-structured thin film. An alternative method is the use of Atomic force microscopy (AFM) which generates a topographical map of sample surfaces and can be used to measure individual particle sizes. Surface roughness is also determined from AFM surface scans with the particular parameter of interest being the RMS variation of the surface height.

Commercial TiO_2 powders are available in particle sizes ranging from the nano- to micro-scale. The powders cannot directly adhere to a substrate without first being combined in a mixture with at least one aqueous solvent, often with other additives. The solvents and additives need to promote the dispersion of the particles by acting to prevent aggregation, agglomeration, and sedimentation.

For suspensions produced from powders, milling and/or sonication are usually required to break apart any aggregates that form when the powder is mixed with liquids.

Figure 2 shows an example of a particle size distribution as a percentage of total volume for various milling times of a suspension containing 15 vol% of TiO_2 particles suspended in water [8]. The nature of the milling equipment and the milling speed largely determine the

effectiveness of attrition milling. Actual results can vary significantly with variations in the equipment.

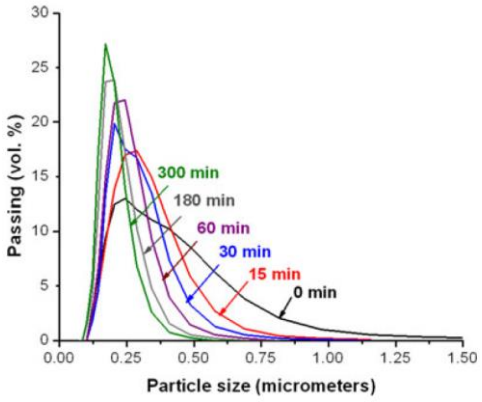

Figure 2: Volume percentage of particle size with respect to milling time [8].

The pore volume of a TiO_2 film is determined by the solvents and pore-forming agents in the suspension; the agents create physical separation between particles and are later driven out through thermal processing. TiO_2 films with a large pore volume can further increase the surface area of the photo-anode.

In the present study, use of Poly ethylene glycol (PEG) and ethanol as dispersion stabilizing additives was explored. The means by which these two additives promote stability are different and the combination of the two can serve to complement each other.

PEGs increase the pore-volume of TiO_2 layers to a degree determined by the molecular weight of the PEG. When added to a TiO_2 suspension the PEG molecules act as a surfactant, coating TiO_2 particles and providing physical spacing between them. As PEG molecules decompose completely at low temperatures, they have become a popular choice as a surfactant and pore-forming agent [9, 15]. See Appendix D for a further discussion of TiO_2 suspension stability and of the properties of PEG and ethanol.

1.2.2 Deposition Methods for TiO_2

Many methods have been used for the deposition of TiO_2 suspensions. Appendix C provides details on the most commonly used methods: dip-coating, screen-printing, spin coating, and doctor-blade. A relatively new approach to TiO_2 depositions is the use of inkjet printing. Inkjet printing allows for the possibility of precisely tailoring the layer thickness and patterning. The literature pertaining to inkjet depositions of TiO_2 has focused on depositions of TiO_2 suspensions for the formation of TiO_2 layers with a uniform density [8-22]. No consistent TiO_2 suspension formulations have been reported for inkjet printing with the exception of Deionized (DI) water as a primary solvent. Beyond that commonality, many different additives, co-solvents, and particle loading levels have been used.

The primary features required for a commercial inkjet printer suitable for printing TiO_2 suspensions are the presence of a piezoelectric printhead, the availability of an ink storage cartridge able to be loaded with a custom solution, and the ability to print directly onto a substrate. Appendix C, section C.2 provides more information on the differences in inkjet printing systems. Several different manufacturers produce printers which feature a piezoelectric printhead, notably Epson, all of whose printers feature with permanent piezoelectric printheads.

A number of options are available for loading custom inks and other solutions including refillable ink tanks and continuous ink supply (CIS) systems that have a high capacity external reservoir that connects to installed ink cartridges via feed lines. Most printers employ a paper feed system that is not readily adaptable for printing onto thick, rigid substrates. Exceptions are those printers with direct CD printing capability or have optional feed trays for printing on items such as plastic ID cards.

1.3 Solar Cell Performance Assessments

The performance of any solar cell is judged by the cell's current and voltage relationship as represented by the cell's I-V curve. One way to generate an I-V curve for a solar cell is to connect a variable resistive load to the cell. By varying the resistance of the load from 0 to an open-circuit level, the voltage across the cell increases to a maximum level, the open-circuit voltage (V_{oc}), and in turn the current through the cell, starting at a maximum level, the short-circuit current (I_{sc}), falls to zero.

For a given resistance value, the voltage and current measurements supply the coordinates for the I-V curve with current on the y-axis and voltage on the x-axis. At some point on the curve, the product of the current and voltage reaches a maximum value. This is the maximum power (P_{max}) point of the cell. Ideally this point would correspond to the product of I_{sc} and V_{oc}. The basic features of an I-V curve are shown in Figure 3.

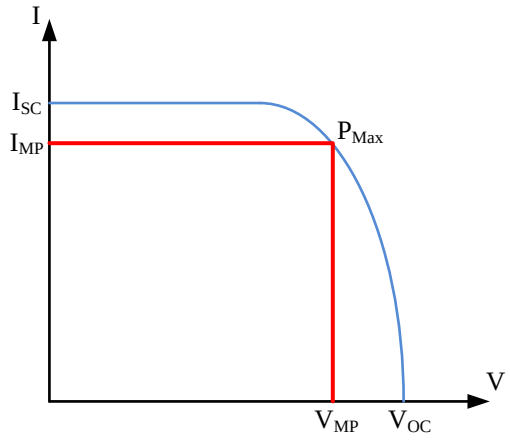

Figure 3: A representative I-V curve for a solar cell.

The Fill Factor of a solar cell is a measure often used to relate these values according to the relationship in Equation 1-1:

$$FF = \frac{I_{MP}V_{MP}}{I_{sc}V_{oc}} \qquad (1\text{-}1).$$

The Fill Factor of a solar cell is a useful comparison between the maximum power obtained from the cell and the power available if there were no internal power losses in the cell. Real cells always lose some measure of power to the effects of shunt and series resistance. The value of the Fill Factor can thus give an indication of the performance of the cell compared to the ideal case.

The shape of the I-V can also provide an indication of which type of resistance is in evidence with the device: with increasing series resistance the value of V_{MP} decreases; with increasing shunt resistance the value of I_{MP} decreases. I-V curves are generally summarized by the reporting of the Fill Factor, I_{sc}, and V_{oc}.

1.4 Summary

Even though standard dye sensitized solar cells have a reasonably simple structure, their ability to convert solar energy into electrical currents is governed by a number of complex interface reactions. The reaction with the lowest overall efficiency effectively determines the overall device efficiency. To achieve general acceptance as a viable alternative to silicon solar cells, DSSCs must achieve higher performance

The semiconductor layer in a DSSC is typically comprised of a nano-structured metal oxide, most often TiO_2. Properties of a TiO_2 layer, including the particle sizes and porosity, are among the most significant determiners of device performance. These properties affect the amount of photosensitive dye that can be loaded onto the layer and also the conductivity of the layer. Of the many methods to deposit TiO_2 films, inkjet printing offers to potential to gain better control over the deposition process and of the resulting characteristics of deposited TiO_2 films.

2 Problem Statement and Hypothesis

The general goal of this research project was to explore possible means of improving DSSC performance. In pursuit of this goal, two principal objectives were formulated: 1) improve the TiO_2 deposition process through the use of inkjet printing and 2) improve DSSC performance by enhancing characteristics of deposited TiO_2 films. Inkjet printing of TiO_2 offers several avenues for potential improvement over alternative methods including more efficient material usage, increased control over material placement, and versatility in TiO_2 film composition. The properties of a DSSC's TiO_2 film in a DSSC are of vital consequence to the overall device performance; improving the structural design of the film can directly improve the cell performance.

A primary research focus was on the deposition of a novel TiO_2 film structure using inkjet printing. The form of the structure was based on the hypothesis that a TiO_2 film with a graded density profile would improve DSSC cell performance.

2.1 Approach

It is well established that a thin, highly dense layer of TiO_2 nanoparticles deposited prior to adding a thicker and more porous layer can directly enhance DSSC performance [1, 6-7, 10]. What has not been explored is the effect of introducing additional layers to more finely grade the entire TiO_2 film with a density profile that progresses from high to low. A high density on the substrate surface improves electron transfer. While a graded density profile in the interior of the film would be expected to improve the film conductivity. And finally, a low density on the upper surface would allow for a large surface area at the primary electrolyte interface. Inkjet printing as a method of depositing TiO_2 suspensions is well suited for such a scheme, particularly if the system has a multi-ink supply system.

Two ways of creating variations in TiO_2 film density are adjusting particle size and varying the pore-forming agents present in the TiO_2 suspension prepared for deposition. Thus, to achieve the variations in film density for this project, TiO_2 suspension formulations were required which could produce layers with varied densities.

2.2 Assessment

Improvements in DSSC performance resulting from the graded density TiO_2 film would be expected in two distinct ways. First, it would allow for a reduction in the series resistance between the layer and the TCO substrate. The series resistance reduction would be measureable as a change in the DSSC Fill Factor. Secondly, the density grading would create an increase in the current generation versus a film with a moderate, uniform density. This would cause an increase in the short-circuit current.

For the assessment of the graded density's effect on device performance, the Fill Factor and short-circuit current were the main parameters of interest for this study and were compared to devices with a uniform density and with two density regions. The assessment of inkjet printing effectiveness as a deposition method was based on a comparison of DSSC performance with printed TiO_2 films versus spin-coated films.

2.3 Research Objectives

The starting objective for the research was to develop a means of producing TiO_2 films with varied densities. The approach chosen was to develop multiple TiO_2 suspensions with a range of particle sizes and pore-forming additives of varying molecular weight. The former would directly affect the density and the later would alter density by changing the pore volume.

A secondary objective was to use inkjet printing as a means to deposit multiple suspensions in sequence to create the graded density in the deposited TiO2 films. This objective

was motivated by a lack of reports concerning inkjet printed TiO_2 layers with anything other than a uniform composition of particle sizes and with a consistent density. Table 1 lists the specific tasks undertaken to achieve the research objectives.

Table 1: Specific tasks and activities required to pursue the research objectives

	Research Tasks
1	Select and modify an inkjet printer for TiO_2 suspension deposition
2	Develop method to produce particle size variations
3	Develop preparation methods to produce suspensions for printing and spin coating
4	Verify that suspension composition affects layer density
5	Produce inkjet printed and spin-coated samples and determine surface properties
6	Assemble and test DSSCs with inkjet printed and spin-coated TiO_2 photoelectrodes.

3 Experimental Setup and Analysis Methodology

An inkjet printer was selected with the required characteristics of substrate compatibility, suspension loading, and accessibility of system components for maintenance and cleaning. Once obtained, the printer required several modifications in order to print non-standard inks. An important next step was to develop procedures to ensure that particle sizes were within printable ranges.

Based on a review of the relevant literature [8-31], several suspension formulations and preparation procedures were developed with fluid properties appropriate for the specific deposition methods of spin-coating and inkjet printing. The development of suitable suspensions for inkjet printing involved assessing the suspensions for long and short term stability against particle aggregation. Atomic force microscopy (AFM) and Scanning electron microscopy (SEM) analysis methods were developed to assess characteristics of the final film layers.

3.1 Printer Selection

There were several options for a suitable inkjet printer. The preference in the printer selection was for a commercial inkjet printer to be used due to the significantly lower costs versus a high-grade research printer or a custom built machine.

After a review of the available commercial printers, the Epson Artisan 730 multi-function inkjet printer was selected for initial testing. The Artisan 730 features a 6-ink piezoelectric printhead with 180 nozzles per color; each nozzle having a diameter of approximately 20 μm. Ink tanks are identified by color: black, yellow, light and standard cyan, and light and standard magenta. Refillable ink tanks for pigment based inks were obtained to replace the OEM supplied pre-filled ink tanks. These ink tanks possessed a reset chip which resets to a full reading when removed and reinserted. CD/DVD printing is an included feature of the Artisan 730, allowing for

the loading of a CD-sized substrate holder for direct printing. A holding tray for CD printing extends out for loading and retracts for printing. Attempts to print onto glass substrates without a substrate holder proved impossible as the glass would slide out of position during loading.

A substrate holder was created from 2mm thick plastic shaped and sized identically to a standard CD. One inch square cutouts in the holder accommodated 1x1in substrates held in place by tape. The substrate holder could accommodate eight substrates but the maximum size of each was limited to 1.5 in square substrates due to the size of the loading tray. With the substrate holder securing the glass slides, no jamming occurred during loading or printing.

Included CD/DVD printing software allowed for precise positioning of printed areas; using the software, solid colored squares were aligned to the cutouts of the substrate holder. For preliminary characterizations, the printed areas were 1cm by 1cm centered on the positions of the substrates. The color selection used for the squares determined which combination of ink tanks were used in the printing. Black and yellow proved the easiest to isolate completely but suitable colors were established for isolation of the individual blue and magenta tanks.

3.1.1 Ink Path

Unlike some other models of printer, the Artisan 730 has stationary ink tanks that do not travel with the printhead. Ink is supplied from the tanks to the print head through six feed lines, one for each color, that are approximately 20 cm in length. This imposes a minimal requirement on the volume of a suspension to be printed of approximately 3ml in total: 1 ml for filling the feed line and 2 ml for satisfying the minimal ink level requirement. The ink tanks are positioned directly above inlets that supply the feed lines to the printhead module. Reservoirs inside the printhead module and behind the nozzles hold a quantity of ink in readiness to refill the printhead after a droplet is jetted.

3.1.2 Printer Modifications

The Artisan 730 includes a flatbed scanner for copying and document scanning, which was detached from the main unit to facilitate access to the ink tank area and to the print head. This required disabling sensors that prevents operation of the printer with an open lid. Removing the scanner and disabling the lid sensor constituted the sole physical modification of the printer. During ink path cleaning, the printhead was removed for soaking in a cleaning solution; feed lines and ink tank inlet were isolated for a forced fluid purge using deionized water and ethanol.

3.2 Spin-Coating System

The spin-coater used was a SRC laboratory spin coater, capable of spin speeds up to 3000 RPM. A spin cycle with the SRC coater is fully programmable to include multiple ramping sequences to control the thickness and drying time of spun layers. Substrates are held in place during spinning by a vacuum system. For sample preparations, TiO_2 suspensions were dropped onto substrates with a stainless steel spreader and immediately spun. The programmed spin cycle began with a 3 second spin period at 100 RPM followed by a 3 second ramp to 3000 RPM. The cycle was held at 3000 RPM for a period of 20 seconds. The entire spin cycle provided sufficient time for the deposited suspensions to have fully dried.

3.3 Milling Apparatus

To improve the breakup of TiO_2 particles and aggregates, a milling apparatus was constructed. The apparatus as assembled consists of three primary elements: the milling jar, a rotating carriage to support the jar, and a variable speed bench grinder to drive the rotation of the jar. An alumina jar with a 100 mL capacity was selected as the grinding jar. Fifteen 10mm diameter ceramic balls and forty 5mm balls were supplied with the jar. Once loaded with a

suspension, the jar was placed into the carriage and clamped in place with 3 screws. A simple coupling provided the connection point with the grinder for rotation.

The bench grinder, a 3" multipurpose grinder manufactured by Central Machinery, has a listed spin speed up to 10,000RPM when unloaded. A tachometer was used to verify the spin speed when driving the rotation of a loaded grinding jar. An adjustable braking method using applied friction was used to maintain the rotational speed between 100-250 RPM.

Figure 4 shows the assembled apparatus as it was used for the preparation of suspension samples.

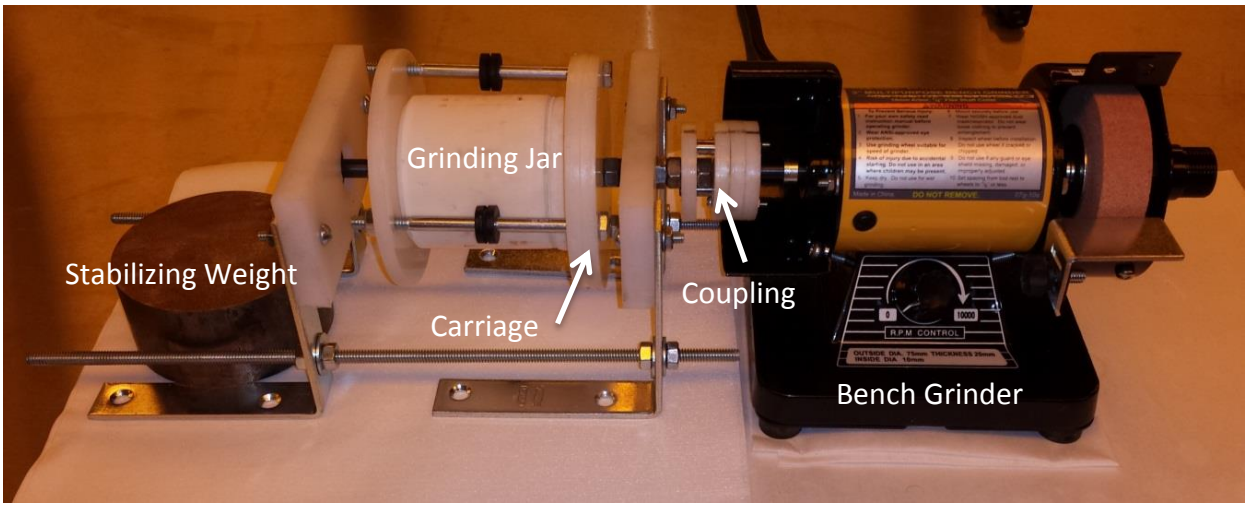

Figure 4: Suspension milling apparatus. The milling jar is shown in place within the carriage.

3.4 Titanium Dioxide Suspension Development

A number of suspension formulations were prepared with variations in the concentrations of TiO_2 particles, ethanol and poly ethylene glycol. Upon preparation completion, suspensions were placed into a sample beaker. After two weeks at room temperature the suspension dispersion stability was assessed. The characteristics of interest were the level of the sedimentation collected at the bottom the beaker and the height of the main volume of dispersed particles. For stability testing of low-viscosity suspensions, the preparation included a milling

period of either 60 or 120 minutes as a means of mechanically breaking down large particles and aggregates.

Two supplies of TiO_2 particles were available for inclusion into suspensions: VP Aeroperl and Aeroxide both from Evonik Industries (Degussa). The Aeroperl are specified by the manufacturer as having particles with an average size of 20µm and the Aeroxide particles have a typical size of 21nm.

Suspensions were prepared with some combination of deionized water obtained through a deionizing system, poly ethylene glycol as received from Sigma Aldrich in 20,000 g/mol (BioUltra 20000) and 600 g/mol (BioUltra 600) molecular weights, and Anhydrous alcohol reagent (Photrex Reagent from J. T. Baker). The alcohol reagent was a formulation of formula 3A denatured alcohol (100:5 mixture of 200-proof ethanol to methanol) with 5% isopropyl alcohol.

Adjustments of suspension pH were achieved with 0.01 M Acetic Acid or diluted 29% Ammonium Hydroxide (J. T. Baker). Either Aeroperl or Aeroxide TiO_2 nanoparticles were used in all suspensions.

3.4.1 PEG Variations

The effect of PEG concentration on the suspension dispersion stability of both types of TiO_2 particles was explored. For comparison, an initial suspension was prepared without a PEG component, DI water adjusted to an initial pH of 3.5 with Acetic acid and 2% of total suspension weight was the 20µm average sized TiO_2 particles. The suspension was thoroughly mixed and subjected to milling for a period of 60 minutes at 250 rpm. Once preparation was complete, the suspension was sealed in a storage beaker.

Within 30 minutes of suspension preparation a line layer of sediment was observed forming on the bottom of the storage container. The sediment was highly viscous but could be readily dispersed by a minimal amount of stirring. Two weeks following the suspension preparation, the sediment layer had thickened sustainably while the upper region, the bulk of the suspension volume, became significantly clearer as shown in Figure 5.

Figure 5: Two week old suspension with no PEG component. A relatively thick sediment layer formed on the bottom of the storage beaker indicating poor stability. The height of the sediment observed in the sample was measured to be 15% of the total height of the suspension.

Using the same initial suspension formulation, PEG600 and PEG20000 was added in varied proportion to the amount of TiO_2. For each suspension variation the sediment height, when measureable, was recorded two weeks after suspension preparation.

Some sedimentation occurred for all suspensions, possibly due to variations in room temperature over the two week storage period or due to a small level of surface level evaporation of the solvent. Most of the prepared suspensions exhibited a gradual decline of the particle concentration near the surface when placed and sealed into a storage beaker.

The suspension variations, deposited onto substrates, were assessed for uniformity and substrate adhesion. This was accomplished by dropping a small sample of a suspension onto an ITO slide and then sintering at 450℃ for 30 minutes.

The results are tabulated in Table 2.

Table 2: Suspension dispersion stability based on varied PEG concentration. The stability of the suspension was assessed in terms of the sediment height relative to the total suspension height. Also noted was the substrate adhesion quality for each PEG concentration.

Poly Ethylene Glycol Suspension Loading Assessment			
PEG600			
% of TiO_2 wt.	PEG wt. (grams)	Sediment Height	Substrate Adhesion
10	0.06	8%	Good
20	0.11	5%	Good
50	0.27	5%	Good
100	0.55	2%	Fair
150	0.82	<1%	Moderate
PEG20000			
% of TiO_2 wt.	PEG wt. (grams)	Sediment Height	Substrate Adhesion
10	0.06	3%	Good
20	0.11	2%	Good
50	0.25	<1%	Fair
100	0.51	<1%	Poor

For PEG concentrations greater than 50% by weight of the TiO_2 loading, the deposited layers showed a propensity to dislodge from the substrate surface. This effect was more pronounced with the PEG20000. In terms of overall dispersion stability, the PEG20000 was more effective in maintaining a high degree of dispersion.

At lower concentrations of PEG the coffee ring effect was notable in deposited drops. Figure 6 shows examples of the coffee rings observed for different concentrations of PEG20000.

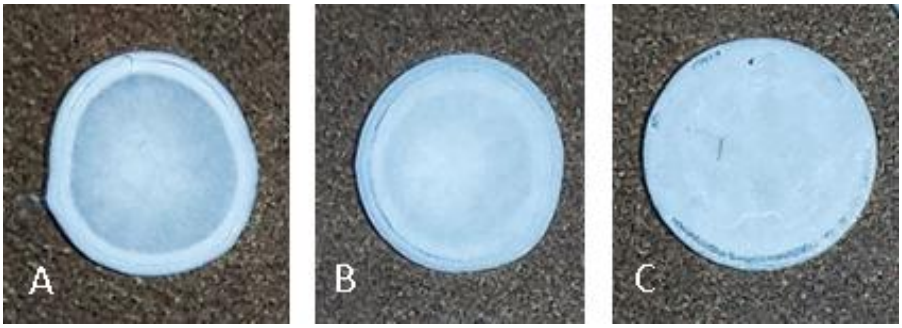

Figure 6: Coffee ring effect observed in deposited drops for different concentrations by weight of PEG20000 relative to TiO_2: A) 10%, B) 20%, and C) 50%

For the lower concentrations of 10 and 20%, the outer edges of the ring were pronounced. Once the concentration reached 50%, the drop was more uniform in distribution but often exhibited weak adhesion to the substrate near the edges. Based on the observations, a concentration between 45 and 50% of PEG relative to the weight of the TiO_2 was used for all suspensions prepared for deposition by printing and spin coating.

A suspension prepared with Aeroxide nanoparticles at 2% vol, DI water adjusted to pH 3.75, and 50% of PEG600 relative to the weight of the TiO_2. Within two hours following preparation, a thin sediment layer developed to a thickness less than 1% of the suspension height. After two weeks, the layer did not substantially thicken and the main suspension volume showed good dispersion, with a slight thinning near the top, as shown in Figure 7.

Figure 7: Two week old nanoparticle TiO_2 suspension, pH adjusted DI water, and PEG600 equal to at 50% the weight of the TiO_2. Dispersion in the main volume of the suspension was maintained.

3.4.2 Ethanol Concentration Variations

To study the effect of ethanol concentration on the suspension stability, a suspension was prepared with a solution of pH adjusted DI water as the main solvent, the 21nm average sized TiO_2 particles 2% of total suspension weight, and 20% Ethanol added in the form of the Photrex reagent. Using the 21nm TiO_2 particles, only a thin layer of sedimentation was observed and, as shown in Figure 8, the dispersion of the particles was observed to be superior in comparison with the suspension with no Ethanol (Figure 5).

Figure 8: Two week old suspension with 20% Ethanol by vol., 2% TiO_2 by wt., and pH adjusted DI water as the primary solvent. Sediment layer on the bottom of the beaker was observed to be less than 1% of total volume.

Increasing the ethanol concentration beyond 20% did not significantly improve the dispersion stability. At a concentration of 80% ethanol by volume, the stability of the suspension decreased and a thicker layer of sediment formed on the bottom of the storage beaker as shown in Figure 9.

Figure 9: Two week old sample with an 80% ethanol content. The bottom sediment layer is thicker than the 20% content, indicating an acceleration of sedimentation. The upper region shows a nearly uniform distribution.

Adding both Ethanol and PEG resulted in suspensions with the lowest sedimentation levels and the highest degree of maintained dispersion following a two week period. Figure 10 shows a two-week old suspension prepared with DI water pH adjusted to 3.56 with acetic acid, 10% by vol. Ethanol, 2% by vol. 20μm TiO_2 particles, and PEG20000 at 50% of TiO_2 weight. The PEG was added after a two hour milling period.

Figure 10: TiO_2 suspension two weeks after preparation that began with 20µm TiO_2 particles and incorporated both ethanol and PEG20000. Preparation included 2 hours of milling.

The presence of ethanol in the suspension solution was observed to influence the surface level morphology. Without ethanol as a co-solvent, the minimum particle sizes detectable at the surface of a printed layer were approximately 50 nm with a root mean square surface height of 18.8 nm. Addition of ethanol reduced minimum particle sizes to 30 nm and increased the surface roughness to 27.1 nm.

Figure 11 shows an example of an AFM scan line for a TiO_2 film prepared from a suspension without ethanol. An example of an AFM scan line for a TiO_2 film using a suspension that incorporated ethanol as a co-solvent is shown in Figure 12.

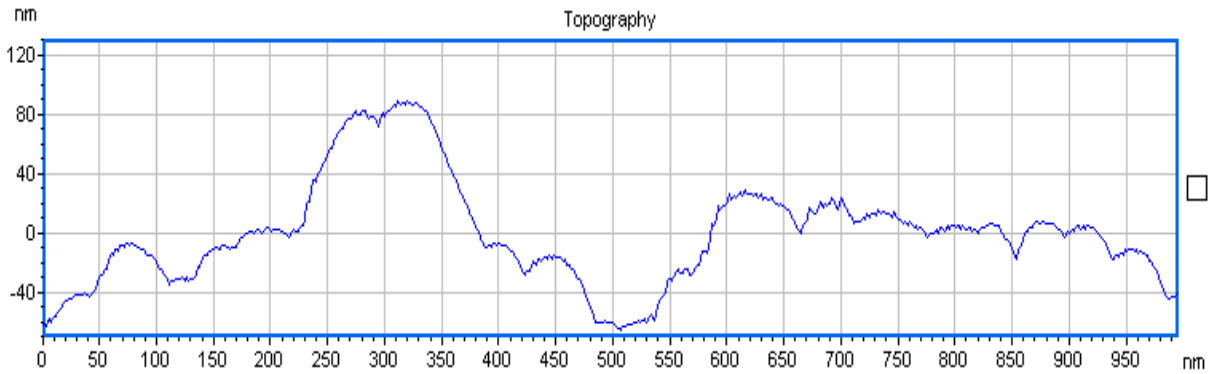

Figure 11: AFM scan line of a TiO_2 film formed from a suspension without an ethanol co-solvent.

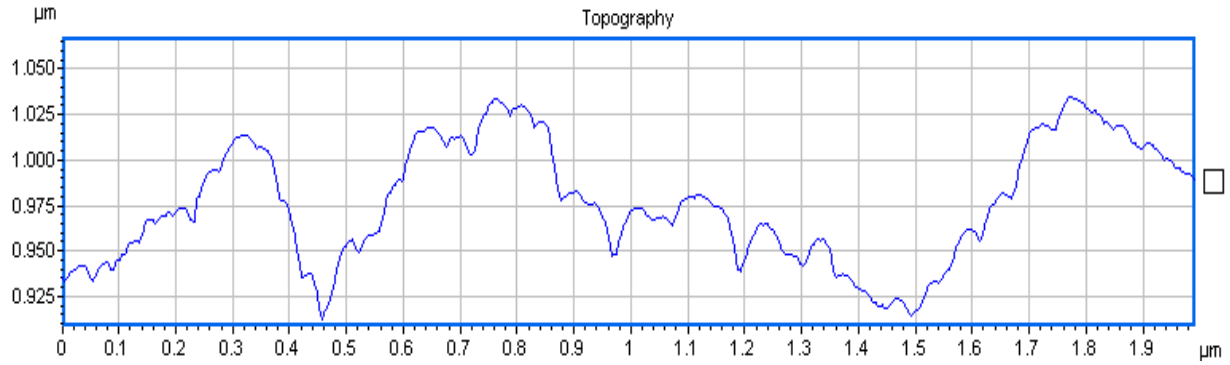

Figure 12: Including ethanol in the suspension formula helped to reduce the particle size and also increased the porosity of the surface layer.

The effect of the ethanol was seen to promote separation amongst adjacent particles and to also increase the overall surface roughness. In Figure 11 above, the particles are generally clumped together to a higher degree than the surface shown in Figure 12 and as a result, the effective particle size in the suspension prepared with ethanol is in the range of 25-50nm whereas the suspension without ethanol is greater than 50nm.

3.5 Suspension Filtering

Mill times of 60 minutes were used with nanoparticle suspensions prior to the addition of PEG. When forming suspensions using TiO_2 nanoparticles, aggregates did not develop as extensively or as quickly as did with the micron particle suspensions. After adding the PEG and mixing thoroughly, another 30 minutes of milling was used to ensure that any particle aggregations resulting from PEG addition would be broken up. SEM and AFM surface scans were able to establish that the layers were largely free of surface aggregates.

Two filtering techniques were used to eliminate large particles and aggregates from suspensions. The first involved allowing the suspension to settle for 24-48 hours such that sediment would form and larger particles would fall further down into the volume. An upper portion of the settled suspension would then be removed and used to deposit a new layer. This type of passive filtering was very effective in reducing the number of micron-sized aggregates

visible on the surface of deposited layers but failed to completely eliminate them. This suggests that while the larger particles and aggregates do tend to drift down in suspension, they are still dispersed to a degree throughout the volume of the suspension.

Filter papers and syringe filters were explored as a means of removing large aggregates from the suspensions. The paper filters were used to retain large particles and aggregates from the entire prepared volume of suspension. Two grades of Whatman filter papers were used for this purpose: grade 93 and grade 5. Grade 93 retains particles 10μm in size and larger; grade 5 retains particles 2.5μm in size and larger. The paper filters were used in sequence to help speed up the filtration time.

Syringe filters allowed for a much finer sifting of the suspension prior to insertion into ink tanks by providing particle filtration to sizes below 0.45 and 0.2μm. The syringe filtering resulted in suspensions that were free of large particles and aggregates.

3.6 SEM Particle Size Methodology

For each TiO_2 film sample deposited onto ITO-coated glass, a minimum of three SEM images were obtained at varied locations of the film. The images were analyzed to detect the individual particles and determine their sizes based on the image scale. The analysis was performed using a custom image processing routine developed for the ImageJ software program[1].

The high magnification of the SEM images collected and the fact that TiO_2 is a semiconductor accounted for a relatively low contrast between particle edges with adjacent particles and with the underlying material. The limited contrast inherently limited the overall

[1] ImageJ is a Java-based image processing program originally developed for the National Institutes of Health. The program allows for the development of custom image processing macros and plugins. It is freely available for download at http://rsbweb.nih.gov/ij/.

precision obtainable from the SEM images and allowed for relatively simple image processing routine. The objective of the analysis was essentially confined to establishing trends in the particle sizes with respect to milling time.

Analysis of each image began with preprocessing in order to enable more effective aggregate and agglomerate detection. The preprocessing included several steps beginning with the establishment of the pixel scale with reference to the superimposed scale bar which was imprinted onto the image automatically by the SEM software. The images were then converted from gray scale to binary through a thresholding process, yielding a black and white image. Following the thresholding, the particles appear as white clusters.

Inverting the image converts all of the particles to black on a white background. The next step was to eliminate any particles below a minimum size to help prevent noise in the image from registering as an actual particle. Small particle elimination was done by removing any distinct areas in the image of black shapes with a total area of 4 pixels or less. The particle detection algorithm was then applied with the results showing only the detected perimeters of each particle mass.

The perimeter result was used to identify if individual particles—which appear distinct in the original SEM image—were being incorrectly grouped together and counted as a single larger particle mass. Often the grouping occurred when there was a high contrast difference between the interior and the edge of a particle.

When necessary, areas in the SEM images containing such incorrectly lumped particle masses were manually drawn out of the image. For a typical image the manual removal of problematic areas was necessary to avoid skewing the size distribution towards unrealistically high values.

For the final particle detection, the minimum area threshold was set of an area of $0.02\mu m^2$, corresponding to a circular particle with a diameter of 160nm. A circularity parameter in ImageJ's particle detection plugin was utilized that compared the area to the perimeter length of each detected particle according to the relationship of equation 3-1:

$$Circularity = 4\pi \frac{Area}{Perimeter^2} \tag{3-1}$$

This use of this parameter helped to distinguish individual particles, roughly circular in shape, from aggregates which typically were polygonal in structure. (The size distribution of individual particles was the target of the analysis and not the size of aggregates.)

A value of 0 for circularity indicates an infinitely elongated polygon and a value of 1 is a perfect circle. The allowable circularity for a detected particle was set to the range of 0.02 to 1.00 for this analysis as it proved sufficient to eliminate most aggregates from the particle count. The particles detected by the imaging method were thus distinguished between the aggregates of smaller particles and the larger particles that had been reduced in size from the original micron-sized powder.

A final image was produced showing the areas identified as particles. The pixels enclosed by each area were summed and converted into dimension units based on the scaling factor established at the outset.

Particle areas were tabulated by ImageJ in terms of square microns and the average area, the standard deviation, minimum and maximum were calculated or identified. From the tabulated results, a particle size distribution—based on a calculated diameter under the assumption of full circularity and normalized with the total number of detected particles—was plotted using Microsoft Excel. This was used to track the effect of milling time on the observed particle size distribution.

The analysis did allow for a means of determining if the milling apparatus would be able to produce suspensions with varied particle sizes and if the maximum detected sizes could be shifted to levels within the printable range of the inkjet printhead. The results of the analysis are given in the next section.

Figure 13 shows the images produced as this process was executed for a SEM image.

The sample had been deposited from a suspension milled for 20 minutes following initial mixture. Image A is the original scanned image, B the binary version, C the inverted image of the binary, D show the effects of outlier elimination, E is the detected particle outline, and F is the final image showing the areas detected as particles. For this image, the average particle size was 2.37μm^2 with a maximum detected particle diameter of 11.8μm.

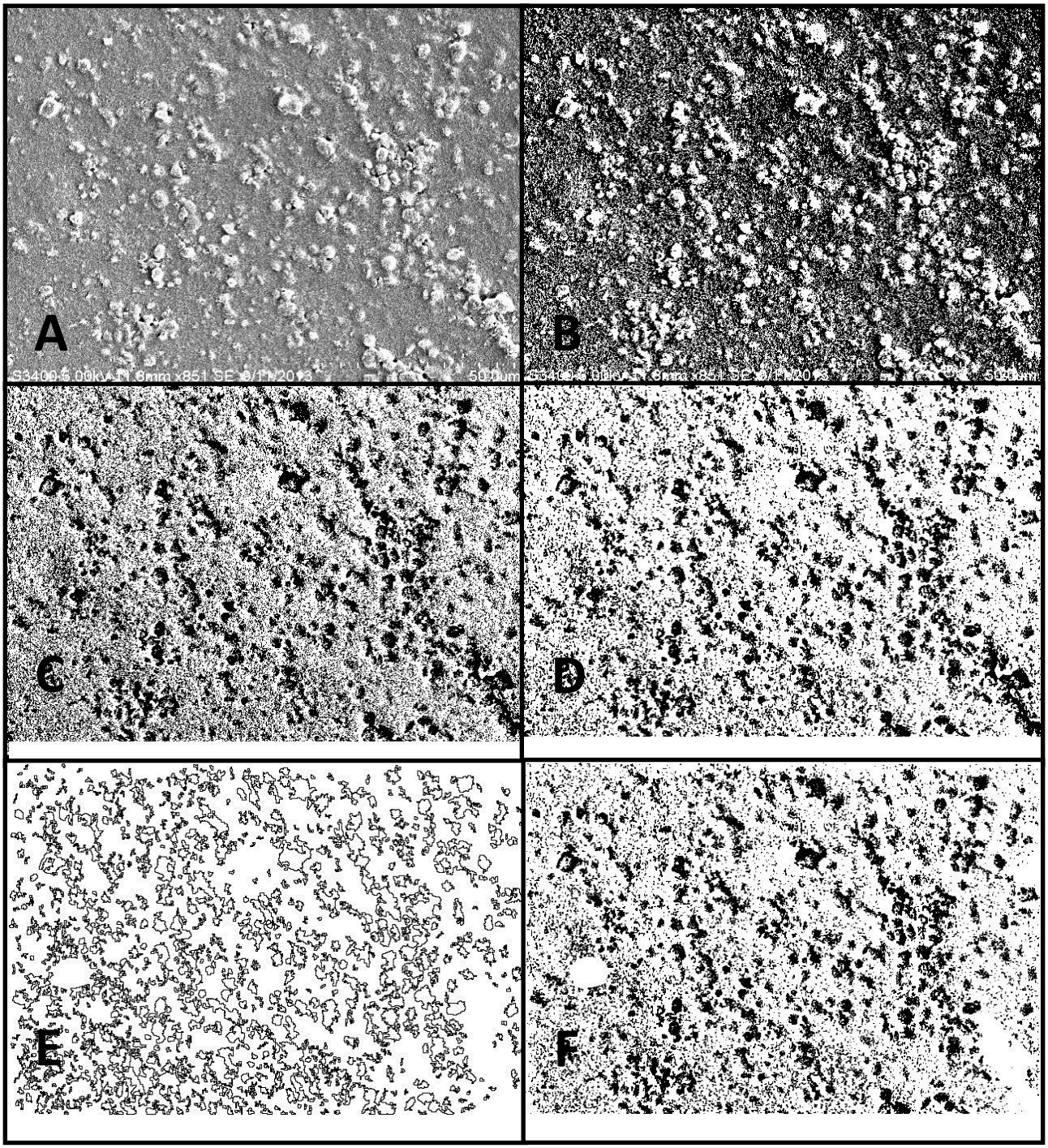

Figure 13: Image analysis process for particle size determination. After setting the image scale, the original image (A) is converted from grayscale to binary (B), the binary image is then inverted (C), and smallest sized outliers are removed (D). The outline view (E) of the particle detection analysis is used to ensure multiple particles are not incorrectly combined. If necessary, some areas of the image are manually cleared to ensure a more accurate analysis. The final image shows only the detected and counted particles.

3.7 AFM Surface Scanning

The difference in the surface morphology of the various TiO_2 preparation methods was quantified through the determination of the surface roughness and the measurement of the pore volume enclosed between the upper portion of a scanned surface and the lowest surface points. These surface parameters were determined through the analysis of AFM surface scans.

3.7.1 AFM System

The AFM system used was the Agilent Technologies 5400AFM with the PicoView and PicoImage Basic software packages. PicoView is the system control program were the scanning mode, probe position, scan speed, resolution, and other parameters are set. PicoImage provides a number of tools to enhance collected images.

All AFM scans were obtained using the AC scanning mode. In this mode the AFM controller uses a drive signal in the form of a sinusoidal voltage to oscillate a silicon cantilever. The frequency of the signal is first tuned to be as near to the resonance frequency of the cantilever as possible, typically around 295 kHz. When brought near the sample surface, the oscillating drive signal causes the probe to lightly tap the surface. The force of the tap can be adjusted by varying the amplitude of the drive signal. Due to the nature of the probe movement when driven by an AC signal, the AC scanning mode is often referred to as Tapping Mode.

3.7.2 AFM Scan Analysis Methodology

The intent for the AFM analysis was to gauge the surface characteristics of continuous sections of the TiO_2 and to exclude features associated with non-uniform surface coating or printing and features that developed during sintering such as cracks or large pits that formed from the outgassing of solvents. These types of features were often not directly visible without magnification.

One of the image operators used for TiO_2 layer scans was a line by line leveling operator which used a least squares method to remove the general slope of a surface that is not perfectly horizontal during scanning. After the leveling, a Gaussian filter was applied to smooth the surface based on a surface waviness analysis to identify any oscillations in the line scans. A threshold of 0.8µm was used as the limit for detected wavelengths.

3.7.2.1 Pore Volume

Each TiO_2 sample was scanned over an area of $5\mu m^2$ or $10\mu m^2$. From the scanned image an area was selected that was as uniform as possible, free of any outlying peaks or pores. In some instances, the dominant portion of the scanned surface area would be a large pore, such as shown in Figure 14, a TiO_2 layer deposited from a suspension without PEG. In this case, inclusion of the center region of the scan would significantly affect the measurement of the volume above the surface.

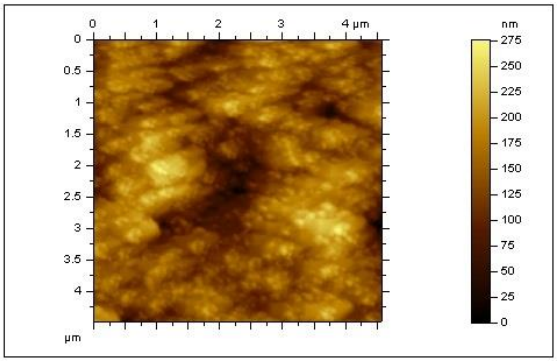

Figure 14: Surface of a TiO_2 layer with a large pore in the central region of the scan.

The presence of a large pore or peak in a scanned area inflates the pore volume enclosed between the top and bottom levels of the surface topography. Figure 15 shows one of the scan lines that cuts through the pore in the center of the area. The lowest point of the pore is over 100 nanometers below the surface level, shown as a solid line.

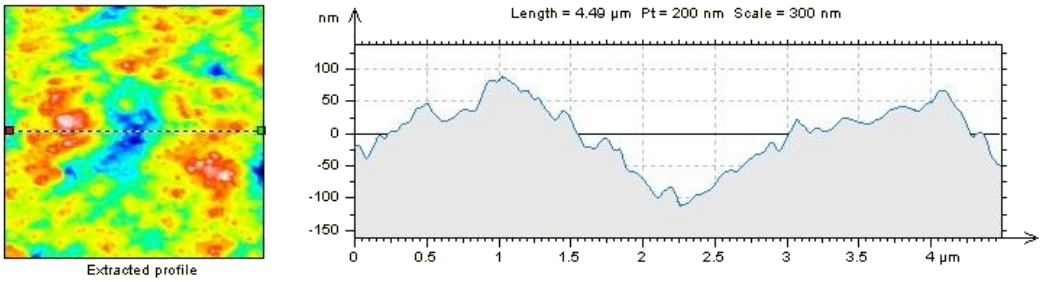

Figure 15: Profile line cutting through pore in the center of the scanned area the previous figure.

Closer to the perimeter of the area the surface appears to have a higher degree of variability in the topography as shown in Figure 16.

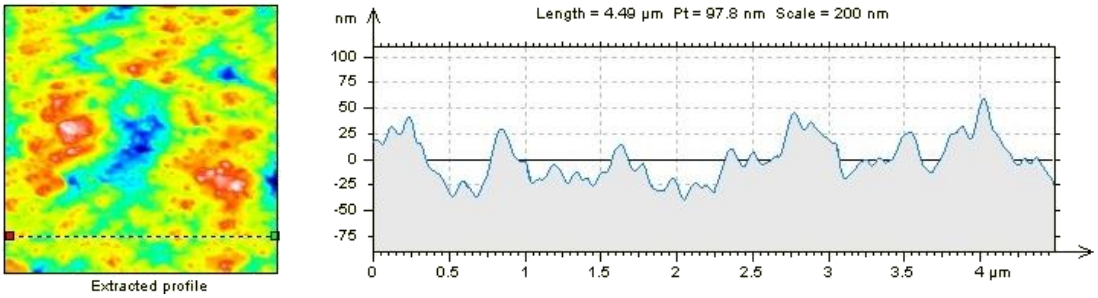

Figure 16: Profile line nearer to the perimeter of the same TiO_2 surface area as Figures 16 and 17. A higher degree of surface variation existed in this region of the scan.

For the purposes of TiO_2 surface characterizations, the areas with large pores or prominent extensions above the surface plane were excluded from the area selected for analysis.

3.7.2.2 Surface Roughness

As surface layers were built up with subsequent depositions via printing or spin-coating, the surface profile range would gradually increase. For comparisons of TiO_2 layers of unequal thicknesses and formed by different deposition methods, the pore volume between the maximum and minimum levels of a scanned surface area proved to be an inconsistent parameter for TiO_2 layers with the identical top level suspension types. In particular, the pore volume measurement did not reliably correspond to the variations in suspension surfactant.

To obtain a consistent measurement for surface comparisons, surface roughness measurements were used. The specific parameter used for the surface measurement was the Root mean square (RMS) surface height.

Scans were first leveled using the least squares method. Then a Gaussian filtered profile was obtained which superimposed a new profile over the original by following the low frequency waves along the surface, effectively flattening the profile of the surface. The PicoImage software refers to this as a waviness operator. An example of the type of profile line this type of analysis produces is shown in Figure 17. Based on the waviness profile, the surface roughness was determined. The advantage of using the Gaussian filtering is that is minimizes the contribution of large scale surface features not related to the actual pore volume of the nano-structured surface.

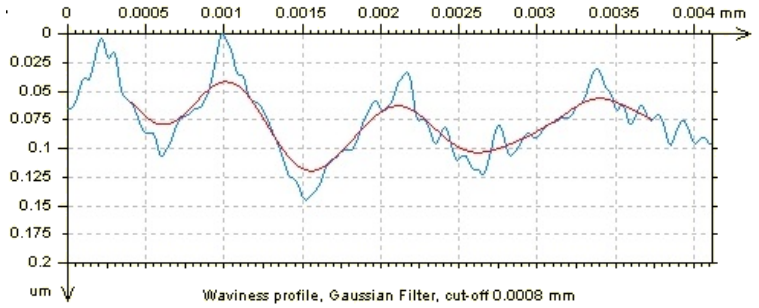

Figure 17: Waviness profile, curved line shown in red, produced by application of a Gaussian Filter on a leveled surface scan profile, shown in blue.

Roughness measurements obtained using the waviness profiles as the surface reference lines were consistent in relation to the surfactant content of the top level of the TiO_2 layer, regardless of the size of the scanned area and thickness of the layer.

4 Layer Assessment and Device Fabrication

4.1 TiO_2 Particle Size Assessment

As one of the proposed approaches to achieving varied density in deposited TiO_2 layers was to utilize different particle sizes, a particle size assessment was required to determine the effectiveness in the grinding of micron size TiO_2 particles. Size assessment relied on SEM imaging of deposited layers and image analysis to assess the particle size distribution. The SEM used was a Hitachi S-3400N.

Suspensions were prepared using varied mill times and with varied chemical formulations. Following preparations, deposited samples would be imaged with the SEM. Gross examinations of the SEM images indicated from the outset that the milling method, regardless of the milling duration, was ineffective in completely eliminating particle sizes outside the printable range.

4.1.1 Deposition Mode Requirements

Depositions by spin-coating did not have restrictions on the maximum particle size in the suspension. A uniform particle size distribution would, however, help prevent deformities in the spun layer. An appropriate suspension viscosity was a critical requirement for spin-coating; for suspensions with high viscosities the coverage was usually incomplete, low viscosities produced excessively thin layers. Spin speeds and spin times required careful adjustment to achieve uniform layers.

Printhead nozzle size in the Epson Artisan 730 is approximately 20 microns [23]. To avoid blockages from developing, the maximum particle size can be no larger than $1/50^{th}$ of the nozzle diameter [18]. The size limitation is discussed in further detail in Appendix C, section C.2.2. This effectively places a 400nm limit on the particle sizes for a printable suspension.

The average particle sizes in stock Epson ink ranges from a low of 58 nanometers for yellow pigments to 157.5 nm for magenta pigments [24]. As Epson print drivers are designed with specific pigment sizes in mind, an optimized suspension formulation would need to match the average particle size of the ink tank being used. This was not attempted for this project. In order to achieve jetting reliability, an upper limit of 250 nanometers for average particle size was set and achieved through the use of filtering.

4.1.2 Micron Particle Size Reduction

The suspensions had to achieve TiO_2 particle dispersion stability and ensure that dispersed particles or aggregates were of an acceptable size. Two methods were explored for the reduction of the micron-sized TiO_2 particles to sizes suitable for inkjet printing: manual grinding and ball milling. Each method was assessed for the production of suitable particle sizes.

Manually grinding Aeroperl particles using a mortar and pedestal was used in initial attempts to reduce the micron-sized TiO_2 particles to the range of 50-200nm. Particles and particle aggregates exceeding the maximum printable sizes were observed in the SEM images of samples prepared using manual grinding. Figure 18 shows an SEM image of a TiO_2 layer deposited from a manually ground suspension with a lower viscosity.

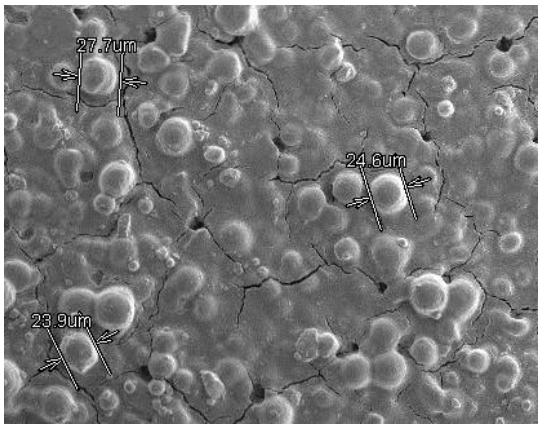

Figure 18: SEM image of a sintered TiO_2 suspension prepared by manual grinding.

The largest measured particle diameter in the sample shown was 27.7 microns. Based on the particle sizes observed with SEM imaging, it was concluded that manual grinding of moderate viscosity suspensions failed to significantly reduce a large portion of the micron sized TiO_2 particles to nano-particles.

Manually ground suspensions also exhibited a high rate of sedimentation, often developing a translucent or clear upper volume after an extended storage period. Figure 19 is an image of a four week old suspension prepared by manually grinding micron sized particles in pH adjusted DI water. Shortly after preparation was completed, this suspension exhibited a high rate of sedimentation.

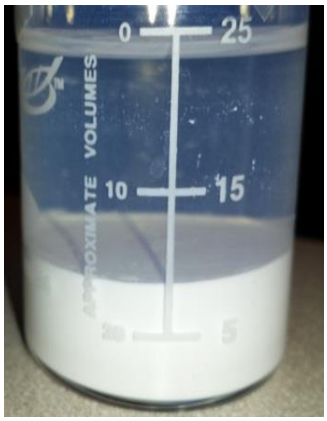

Figure 19: Four week old suspension prepared by manually grinding TiO_2 micron sized particles. The upper volume of the suspension was observed to be nearly transparent.

Two assessment trials to establish a relationship between the milling time of micron-sized particles and the resulting particle sizes. The first trial used a suspension containing PEG600 and the second a suspension containing PEG20000. Both suspension formulations fixed the concentration of ethanol to 10%. A consistent 2:1 ratio of TiO_2 and PEG was also used for both suspensions, with TiO_2 particles at 2% of the total weight. The primary solvent of the suspensions was 0.01M Acetic acid.

Table 3 shows the results for suspensions with PEG600. The average particle size was determined from the entire set of detected particles for a given mill time. The equivalent average diameter is calculated on the assumption of a circular particle. Maximum particle diameter results were based on the largest particle size for a given mill time. The largest observed distinct particle diameter was also recorded for each mill time.

Table 3: Results of the SEM image analysis for detected particle sizes on the surfaces of layers deposited from TiO_2 suspensions containing PEG600.

Particle Size with PEG600 Surfactant				
Mill Time (min)	Average Particle Size (μm^2)	Standard Deviation	Equivalent Average Diameter (μm)	Maximum Particle Diameter (μm)
20	2.32	7.37	1.72	10.7
40	3.23	8.80	2.03	10.6
60	1.51	4.03	1.39	9.3
80	2.15	3.77	1.65	10.9
120	1.07	3.42	1.17	7.76

A general narrowing of the particle size distribution appears to have occurred based on the standard deviation decreasing with increased mill time. A two hour mill time was not sufficient to eliminate large particles completely, although their frequency decreased. Mill times longer than 120 minutes were not attempted given the limitations of the milling apparatus which tended to become unstable during continuous operations exceeding two hours.

These results indicate that the particle size reduction the milling system can achieve, with the milling duration and spin speeds used, is inadequate to produce printable particle sizes. Further, the majority of the particle reduction achieved occurs relatively quickly. The average particle size of an un-milled suspension is approximately 25 microns in diameter, after only 20 minutes this was reduced to 2 microns. Table 4 shows the results for suspensions containing PEG20000.

Table 4: The analysis results for the SEM images of surfaces deposited from TIO_3 containing PEG20000.

Particle Size with PEG20000 Surfactant				
Mill Time (min)	Average Particle Size (μm^2)	Standard Deviation	Equivalent Average Diameter (μm)	Maximum Particle Diameter (μm)
30	1.819	4.90	1.52	7.9
60	1.178	3.71	1.22	7.6
90	0.84	3.28	1.03	7.8
120	1.53	5.14	1.40	8.7

An increase in the standard deviation, average particle size, and largest particle diameter after 120 minutes of milling suggests that the suspensions had become unstable and had begun to allow a faster rate of aggregation.

The particle size distributions with PEG20000 samples also show a failure of the milling to produce average particle sizes below 1 micron further suggesting a limitation in the process. Several aspects of the process could be responsible for the milling being unable to further reduce the particle sizes. Characteristics of the grinding jar or the ceramic grinding balls, such as the cylindrical shape of the jar or the small weight of the balls, may be unsuitable for achieving further size reduction. Another possibility is that the rotation speed needs to be increased to provide more energy to the grinding process.

4.1.3 TiO_2 Nanoparticle Size Assessment

AFM imaging allowed for individual nanoparticles to be measured and an average particle size of 26nm was established. Figure 20 is an example of an AFM surface scan of an inkjet printed sample. The individual particles were distinct and could be directly measured.

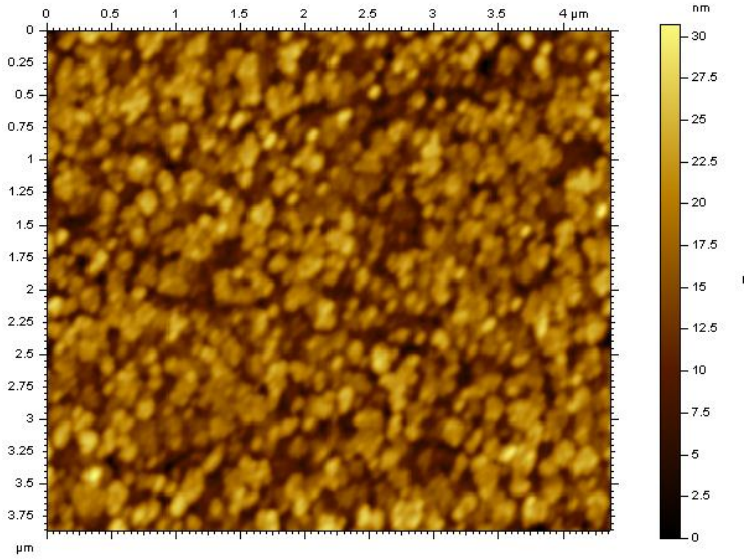

Figure 20: AFM surface scan of inkjet printed TiO_2 film. The average particle size in the sample was determined to be 26.2 nm.

Actual particle sizes ranged from 18 to 50 nanometers. SEM images showed minimal evidence of aggregation, often fewer than 3 or none at all in a 100 micron-sized area. The size and number of observed nano-particle aggregates decreased with increased mill time. To ensure that the majority of aggregates were eliminated from nanoparticle suspensions, filtering methods were used.

4.2 Surfactant Content and Surface Morphology

The secondary means of producing density variations in the deposited TiO_2 films was to vary the surfactant content. As a means to assess the variations in layer morphology based on the surfactant content of deposited samples, SEM and an AFM scans of deposited samples were used.

SEM images were useful in visually examining the surface for micron-scale surface features including the presence of surface cracking, holes, particle clusters, and pore depth. AFM surface scans allowed for an examination of the surface at the submicron scale which allowed for

a surface roughness determination of deposited TiO_2 layers. Topologies from AFM scans were also analyzed to compare the relative difference in surface areas through measurement of the volume enclosed in the space bounded by the surface profile and a plane set by the maximum height of a scanned area.

The surface level assessment of deposited layers intended to provide verification that distinct surface conditions existed for samples with differing top layer suspension depositions. Additionally, a degree of consistency between the surface level characteristics of samples with identical top layer suspension depositions was desired.

4.2.1 SEM Imaging

A Hitachi S-3400N SEM was used to obtain surface images of prepared inkjet printed and spin-coated TiO_2 layers. The samples were deposited onto the conductive side of Indium tin oxide (ITO) coated glass slides. The slides were adhered to an aluminum stage mount with conductive carbon tape. Electron beam energies were set to 15kV; the same magnification scale and image contrast level was generally conformed to for each images.

Figure 21 shows SEM images of TiO_2 layers deposited by inkjet printing. The variation in the suspension compositions used for the deposition of each film was the surfactant/pore-forming agent contribution. In image A of figure 21, the suspension did not include a surfactant, image B included PEG600, and image C included PEG20000. Each of the suspension began with the same initial formulation of 2% by wt. of TiO_2 powder, 28mL of 0.01M acetic acid, and 2mL of denatured alcohol (95% ethanol). The initial mixture was milled for 2 hours and then separated into 3 equal volumes. To one, PEG600 was added in an amount equal to 50% of the TiO_2 weight and to another, PEG20000 was added in the same 1:2 ratio with the TiO_2 powder.

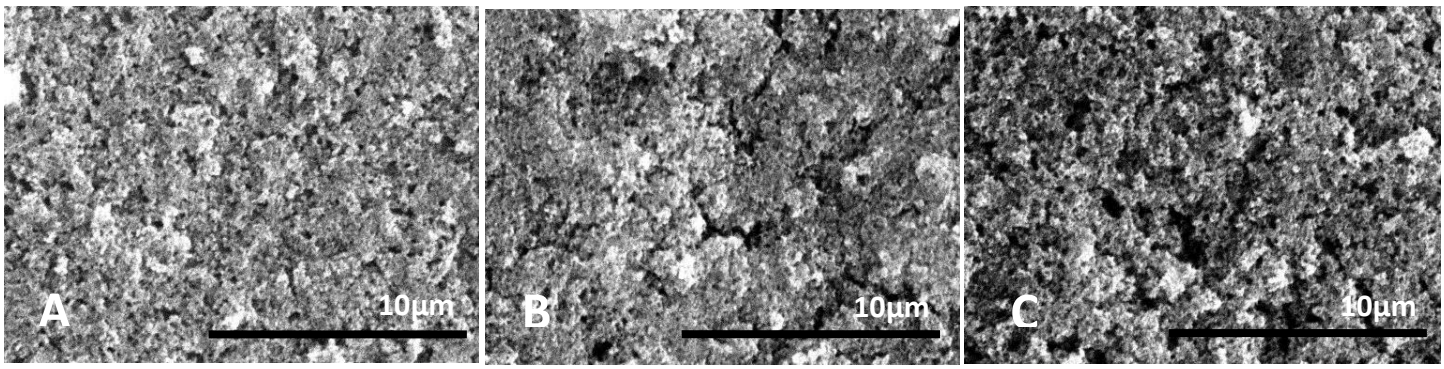

Figure 21: SEM images of inkjet printed surfaces, each with approximate thickness of 5 microns. Image A is of a layer deposited from a suspension formulation of 2% by weight of TIO2 powder and with no PEG; image B of a suspension with an addition of 1% by wt. of PEG600; image C includes 1% by wt. of PEG20000 in the top portion of the layer.

From the SEM images, the porosity of the surface level of the TiO_2 layer is seen to increase with respect to the layer with no PEG added as a surfactant. In image B, the depth and size of the pores have increased, in image C, the number of and sizes of the pores has noticeably increased over the over two samples. Image A and B are of uniform TiO_2 layers formed by successive, overlapping inkjet printing passes.

Layers consisting of uniform printings of the suspension with PEG20000 as a surfactant were found to suffer from poor substrate adhesion when the deposited layer surpassed 2 microns in total thickness. The layer shown in image C used an initial base deposition of the suspension with no PEG and then covered that with a printing of the suspension containing PEG20000.

After each printing pass, the deposited suspension was allowed to dehydrate—indicating that the aqueous solvent had evaporated—before continuing with another printing pass; normally the dying time was within a few seconds of the jetting. The slide was then sintered on a hot plate at 90°C for 10 minutes and then 450°C for 30 minutes.

For the uniform spin-coating of a layer onto a slide, the viscosity of the suspensions was required to be significantly higher than those prepared for inkjet printing. To achieve a higher

viscosity, the TiO_2 and PEG concentrations were increased. The increased levels of PEG were observed to have the more significant impact on the suspension viscosities.

Samples of spin-coated TiO_2 layers were prepared using a similar approach to that used for inkjet printing. Thicker layers were built up by successive coating of an ITO coated glass slide. The area of the photo-anode was defined using tape to limit the coating area to a $1cm^2$ square. After the target thickness was reached, the tape was removed and the slide was sintered using the same temperature and time parameters used for the inkjet printed slides. As before, each deposited layer was allowed to dehydrate prior to applying the next layer.

Figure 22 shows the surfaces of the three spin-coated TiO_2 samples. Image A in the figure is of a layer with no PEG, image B with PEG600, and image C with PEG20000.

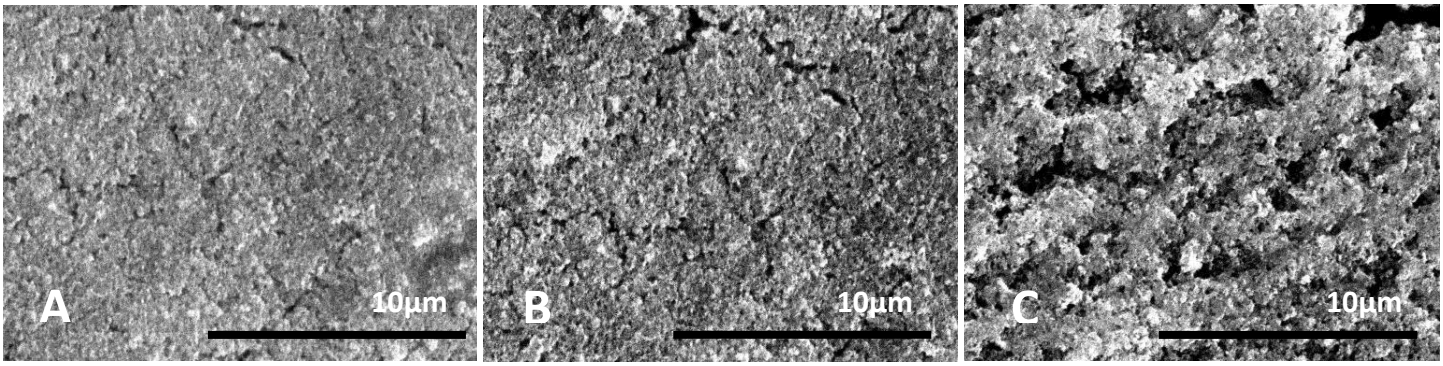

Figure 22: SEM images of TiO2 layers deposited by spin-coating, approximately 5 microns thick. Image A does not include a surfactant; image B includes PEG600 in 1:2 ratio with TiO_2; image C includes PEG 20000 in the same ratio.

One visual difference between the layers formed by spin-coating and those formed by printing was an apparent increase in density at the surface level. Generally, the spin-coated layers possessed an increased amount of material at the surface with a smoother overall appearance than the printed counterparts.

4.2.3 Inkjet Printed Surfaces

The target thickness for the inkjet printed TiO_2 layers was 5 microns, a thickness which required between 5 and 10 printing passes to achieve with the level of TiO_2 concentrations used in the printing suspensions. Reference samples were produced for a uniform composition of the surfactant free suspension and the suspension containing PEG600.

The printing of PEG20000 suspensions was not able to produce a 4-5 micron thick layer without losing adhesion with the substrate. Depositing an initial layer of a surfactant free suspension was normally sufficient to prevent the upper layers from dislodging. Cracking of the surface layer was still an issue with PEG20000 TiO_2 layers but the cracks that did develop were not visible at the macroscopic scale.

Figure 23 shows a surface scan of a uniform TiO_2 layer with no surfactant. The RMS height for this scan area was 28.0nm. The maximum height of the surface was 193nm.

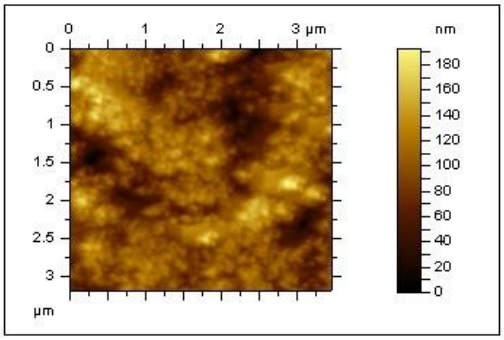

Figure 23: AFM surface scan of a TiO_2 layer with no surfactant content. The RMS height was 28.0nm and the vertical range of the surface profile extended to 193 nm.

For the determination of the pore volume, the region selected used as an upper boundary the plane above which was approximately 5% of the total surface material surface area. The lower boundary was set to the plane which lay above 1% of the material surface area. Figure 24 shows the result of this selection process which returned a value of $0.0445 \mu m \cdot \mu m^2/\mu m^2$ for the pore volume per square micron. The choice of limiting boundary conditions was somewhat

arbitrary; both limits intended to eliminate any outlying peaks and depths. Increasing the lower limit to the minimum 5% of the surface area had a negligible effect on the value determined for the pore volume as most of the volume contribution came from the upper regions.

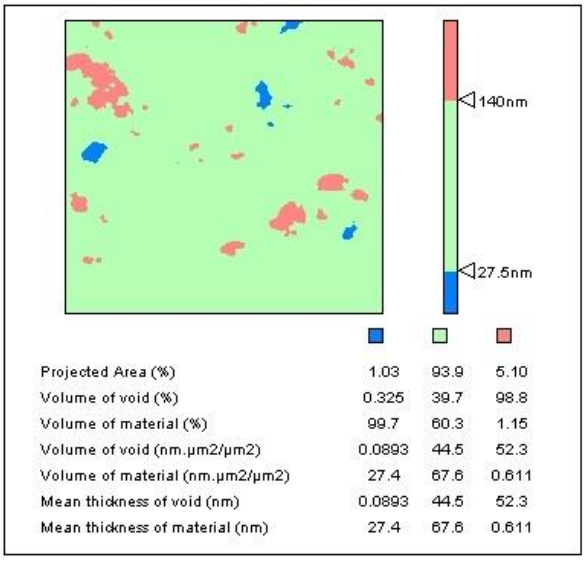

Figure 24: Pore volume determination of the scanned area of Figure 20. Shown are the selected areas of the surface associated with the volume and the parameters obtained from the analysis. The volume of the void parameter, measured to be 0.0445 µm·µm^2/µm^2, corresponds to the enclosed volume between the upper and lower limits.

This analysis was repeated for each of the TiO_2 samples scanned. Figures 25 and 26 are surface scans of TiO_2 layers with surfactant contents of 1% by weight of PEG600 and PEG20000 respectively.

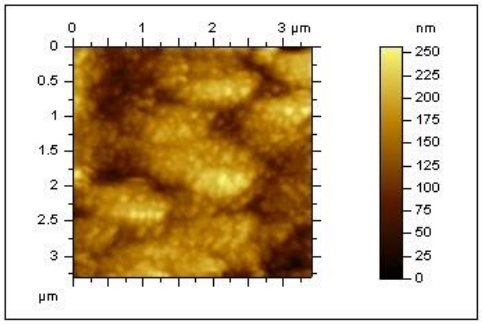

Figure 25: AFM surface scan of a TiO_2 layer with a 1% by weight PEG600 surfactant content.

The surface roughness of the surface, the RMS height, shown in Figure 22 was 40.0nm and the maximum height was 257nm. The pore volume was 0.0627µm·µm^2/µm^2.

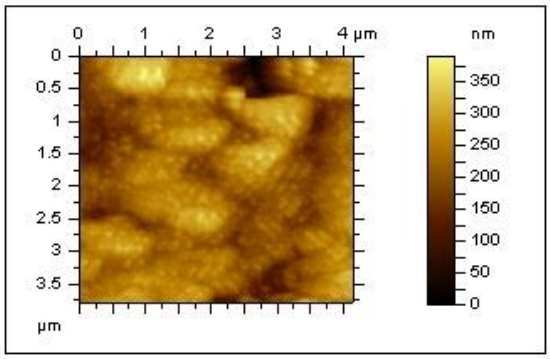

Figure 26: AFM surface scan of a TiO_2 layer with a 1% by weight PEG20000 surfactant content.

For this sample, the RMS height was 52.7nm, the maximum surface height was 391nm, and the pore volume was 0.0777µm·µm^2/µm^2.

The same analysis was repeated for layers of approximately 8 and 1.5 micron thickness. Table 5 summarizes the results of the AFM surface analysis.

Table 5: AFM TiO_2 surface analysis results for different layer thickness and surfactant content for inkjet prepared samples. The samples with no surfactant and with PEG600 were both prepared as successive uniform depositions. The PEG20000 samples required a base layer of the no-surfactant suspension in order to maintain adhesion to the substrate.

Surfactant	Layer Thickness (µm)	Height Range (nm)	RMS Height (nm)	Pore Volume (µm·µm^2/µm^2)
None	8.1	271	31.0	0.073
	4.7	193	28.2	0.0445
	1.4	143	23.6	0.0407
PEG600	8.6	377	37.0	0.097
	4.5	257	40.1	0.0627
	1.5	280	38.4	0.0829
PEG20000	8.7	421	59.5	0.144
	4.3	391	53.7	0.0777
	1.6	327	49.5	0.144

The general trends observed in these measurements were for the height range to increase with layer thickness and the surface roughness to correlate with the surfactant content. The value

of the pore volume did not exhibit a strong pattern. In some cases the thinnest layer of a given surfactant group showed the largest volume.

Samples prepared with top layer depositions different from underlying layers showed surface roughness values—as measured by the RMS height—consistent with those obtained with uniform deposition profiles. Based on all obtained measurements, the range of RMS height values for each surfactant condition is shown in Table 6.

Table 6: Printed average RMS height and standard deviations for each top layer surfactant condition based on all values measured. Data set includes samples with a uniform deposition profile as well as varied deposition sequences.

Surfactant	Average RMS Height (nm)	Standard Deviation
None	27.4	2.7
PEG600	40.4	2.3
PEG20000	57.7	6.9

The increase in the spread of the height for the PEG20000 surfaces stemmed from the measured RMS height values increasing in direct relation to the increasing thickness of the overall TiO_2 film. Part of the increase in surface roughness was attributed to declining droplet volume of the suspension jetted from the printhead. The occurrence of reduced droplet volume was attributed to a gradual accumulation of material at the nozzles causing reduced output, a point returned to in the discussion of printer performance in Section 7.

The basic conclusions of the surface morphology analysis are that increasing molecular weight in the surfactant content does produce a measurable increase in surface roughness, in turn associated with an increase in pore volume and decreasing layer density. Also, the higher the surfactant molecular weight the greater the difference in the overall spread of the surface height.

4.2.4 Spin-coated Surfaces

The overall surface condition of TiO_2 layers deposited by spin-coating was observed to relate directly to suspension uniformity: if the suspension had a suitable viscosity and contained uniformly sized and dispersed particles, the resulting TiO_2 films generally had a very even surface with no significant variations in topography. Table 7 shows the results of AFM surface analysis of spin-coated samples prepared with differing surfactant content. Each sample was the result of two consecutive spin coatings of identical suspensions.

Table 7: AFM TiO_2 surface analysis results for different layer thickness and surfactant content for samples prepared from two spin coatings.

Surfactant	Layer Thickness (µm)	Height Range (nm)	RMS Height (nm)	PoreVolume (µm·µm^2/µm^2)
None	1.8	100	16.0	26.9
PEG600	2.1	164	24.8	43.9
PEG20000	2.3	270	42.2	68.1

As additional layers were spun-on to further develop sample thickness, AFM scans showed a tendency towards increasing surface height variations that were not evenly distributed. Figures 27 and 28, layers of 2.3 and 4.1 microns thick respectively, show an example of this occurrence.

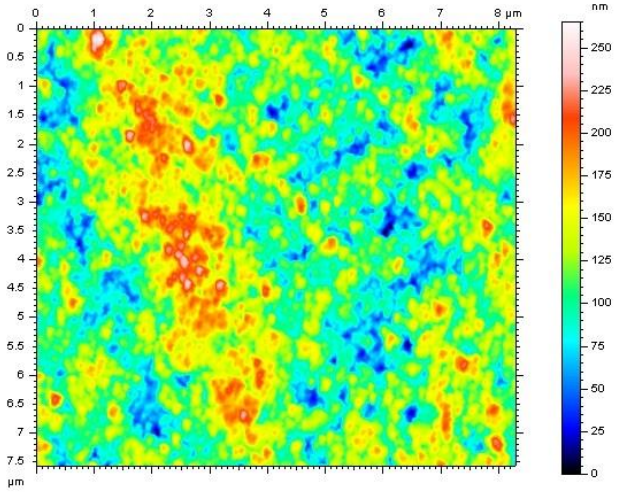

Figure 27: Surface scan of a spin-coated layer of with a top layer suspension with PEG20000 and with 2.3 µm average thickness. The height range in this area was 270nm.

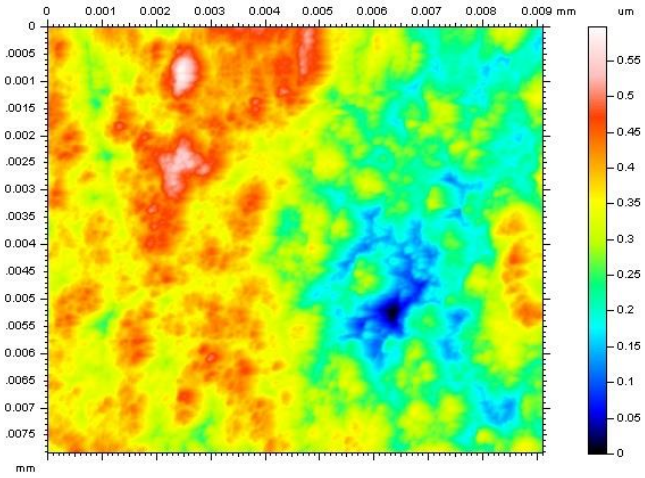

Figure 28: Surface scan of a 4.1 µm thick layer, the surface height range over the area shown is 585nm.

Table 8 shows the average surface level RMS heights in relation to the suspension surfactant of the top layer based on all measurements of spin-coated samples.

Table 8: Spin-coated average RMS height and standard deviations for each top layer surfactant condition based on all values measured. Data set includes samples with a uniform deposition profile as well as varied deposition sequences.

Surfactant	Average RMS Height (nm)	Standard Deviation
None	16.3	2.1
PEG600	26.2	4.3
PEG20000	42.7	3.3

Similar to the inkjet printed samples, the spin-coated films showed an increase in the RMS height of the surface profiles as surfactant was introduced to the suspension formulation. As the molecular weight of the surfactant increased, the roughness also increased. The spread in the measured roughness was less in the case of the high molecular weight suspensions compared to printed films.

4.3 Surface Morphology Conclusion

On the basis of SEM imaging and AFM surface scans, the top level surface morphologies of both spin-coated and printed TiO_2 layers were seen to vary in accordance with the TiO_2

suspension formulation used in the last deposition in the buildup of the sample. Specifically, the surface roughness of leveled and filtered surface profiles correlated to the deposition method and suspension surfactant content: as surfactant was added in increasing molecular weights, the surface roughness increased compared to the surfactant free surfaces. Thus, altering the suspension surfactant content was demonstrated as a means to vary the surface roughness of TiO_2 films. This variation in surface roughness was correlated with changes in the surface pore volume and the layer density.

The pore volume was also seen to generally increase with the thickness of the layer. Comparisons between the surfaces of printed and spin-coated samples showed that spin-coated samples had a smother surface compared to printed layers.

For both inkjet printed and spin-coated samples, the surfactant content in the suspension formulation was validated by the morphology assessments to be capable of successfully producing TiO_2 layers with varied density. On this basis, a number of TiO_2 samples were produced with uniform and varied density profiles based on the surfactant content of the deposited suspensions.

4.4 Suspension Preparation

Suspensions formulated for deposition by inkjet printing or spin-coating contained varying combinations of deionized water obtained through a deionizing system, poly ethylene glycol as received from Sigma Aldrich in 20,000 g/mol (BioUltra 20000) and 600 g/mol (BioUltra 600) molecular weights, and Anhydrous alcohol reagent (Photrex Reagent from J. T. Baker). The alcohol reagent was a formulation of formula 3A denatured alcohol (100:5 mixture of 200-proof ethanol to methanol) with 5% isopropyl alcohol. Adjustments of suspension pH were performed with 0.01 M Acetic Acid or diluted 29% Ammonium Hydroxide (J. T. Baker).

Either Aeroperl or Aeroxide TiO_2 nanoparticles from Evonik Industries (Degussa) were used in all suspensions.

4.4.1 Inkjet Printing

The suspension composition for inkjet printing used deionized water as the main solvent, pH adjusted with 0.01M Acetic Acid to a pH of 3.75, essentially a 0.006M Acetic acid solution. Anhydrous Alcohol reagent, between 1-5% by vol. was added as a stabilizing co-solvent. The TiO_2 particle loading was kept to 2% of the total volume as measured dry. PEG was added in a 45% proportion to the TiO_2 powder by weight.

The suspension processing procedure began with measuring 0.18 grams of TiO_2 powder into a mortar and adding 1mL of the Acetic acid solution. The mixture was hand ground for five minutes before transferring into a milling jar. A premixed solution of the diluted Acetic acid and alcohol reagent (4:1) was added in 5mL increments to the initial mixture, up to a total suspension volume of 40mL. After each addition, the suspension was milled at 250 rpm for five minutes. After adding the full quantity of the aqueous solution, the suspension was milled for an additional 60 minutes.

Two filtering steps were used to eliminate large aggregates from the suspension. Both involved passing the suspension through Whatman filter papers. The first filter paper used was a Whatman Grade 93 filter which retained particles over 10μm, the second filter was a Whatman Grade 5 filter which retained particles over 2.5μm. When the filtering papers were used, the level of initial and long-term sedimentation was substantially reduced.

After filtering, a measured quantity of PEG was added to the suspension and mixed in with a stirring rod if the suspension called for addition of a PEG. The suspension was then

returned to the milling jar and milled for an additional 30 minutes. The inkjet suspension preparation procedures are summarized in Table 9.

Table 9: The materials and processing procedures used for the preparation of a TiO_2 suspension for inkjet printing.

Step	Material Added	Processing Procedure
1	0.18g TiO_2 Powder	Measured into a mortar
2	1 ml 0.0006M Acetic Acid	Grind for 5 minutes then transfer into milling jar
3	5 ml 0.0006M Acetic acid/Ethanol solution	Add in 5 ml increments up to a total suspension volume of 40ml, milling for 5 minutes after each addition
4	--	Two stage filtering process to remove particles 2.5 microns and above in size
5	1ml of 0.08g PEG600/PEG20000	After addition of the PEG, the suspension was thoroughly stirred until fully dissolved
6	--	Final milling period of 30 minutes

4.4.2 Spin-On Deposition

The significant difference between the inkjet suspension and those formulated for the spin-coating process stemmed from the spin-coating requiring higher viscosities in order to obtain complete area coverage. Increases in viscosities were achieved by increasing the proportion of TiO_2 particles relative to the total weight of the entire suspension but still holding the particle weight to an amount lower than the total contribution of the aqueous components. The result was a TiO_2 suspension with a significantly higher viscosity than that used for inkjet printing. As the suspensions formulated for spin-on applications dried, the presence of aggregation and particle clumping would increase, necessitating usage of the suspension shortly after preparation, typically within two days.

After some experimentation, a suspension consisting of 2 grams of TiO_2 powder for each 10 mL of solution was selected. The same solution formulation of DI water pH adjusted with acetic acid used for inkjet printing was employed as the main solvent for spin coating suspensions and was added drop-wise to the powder in a mortar and pedestal. With each

additional drop, the suspension was hand-ground for one minute. Once the full amount of the solution was added, the suspension was transferred into the milling jar and milled for two hours. PEG was added and mixed into the suspension as a final step.

4.5 DSSC Device Assembly

The total area of the deposited layers was kept constant at $1cm^2$ for each sample. For the printed samples this area was defined within the software. For spin-on samples, the coverage area was defined by the use of Scotch tape which was removed after spinning and prior to sintering. The substrate for all depositions was indium tin oxide (ITO) coated glass slides. Each substrate slide was cut from a larger 2x2 inch slide using a diamond scribe to score break lines.

The deposited samples were then sintered on a hot plate, starting at 50°C with a gradual increase to 450°C. The slides remained on the hot plate at the maximum target temperature for 30 minutes. Sintered samples were then immersed into a prepared dye solution containing 0.018mg of Di-tetrabutylammonium cis-bis(isothiocyanato) bis(2,2′-bipyridyl-4,4′-dicarboxylato) ruthenium(II) dye—commonly known as N719—dissolved in 50mL of a 1:1 mixture of anhydrous tert-Butyl alcohol ($C_4H_{10}O$) and anhydrous Acetonitrile (CH_3CN). Once mixed and prior to use, the dye solution was placed on a magnetic stirrer for 3 hours to ensure through dissolution of the dye. All chemicals were obtained from Sigma Aldrich and used as received.

The TiO_2 were kept in the dye solution for a period of 20 hours and then removed and rinsed with DI water followed by IPA. The slides were dried under a light flow of nitrogen gas. Counter electrodes were formed but accumulating carbon soot on an ITO slide by passing the slide multiple times over a candle flame. The iodide electrolyte solution was made by dissolving

0.127g of iodide in 10 ml of ethylene glycol and then adding 0.83g of potassium iodide. This solution was stirred until all particles had completely dissolved into the solution.

The cells were assembled by sandwiching the dye-adsorbed TiO_2 films with the carbon coated counter electrodes with a slight offset of approximately 5mm. Small binder clips were used to hold the two slides tightly together. The offset area allowed for placement of copper tape at the edges of the ITO slides to allow for external connections. The electrolyte was dropped in between the two slides and allowed to completely flow into the interior spaces.

5 Results

Photo-anodes were produced from varied TiO_2 suspensions deposited by inkjet printing and spin coating onto a TCO substrate. An ITO coated substrate was used for both electrodes. On the counter-electrode a layer of carbon, deposited by passing the slide through a candle flame, acted as the catalyst for the regeneration of the electrolyte. An iodide/tri-iodide solution was used for the electrolyte. Assembled cells were held together with binders and copper tape adhered to uncovered areas of the TCO substrate helped facilitate electrical connection to external circuits for DSSC performance testing.

5.1 DSSC Device Assessments

Among the variations were different thicknesses of TiO_2 films produced from consecutive printing passes or, alternatively, by additional spin-on applications of the same suspensions. These resulted in TiO_2 films with a uniform composition and a uniform density profile. Several density profile variations were also made. Some of these variations did not result in viable films or resulted in films with poor surface characteristics such as extensive cracking or material loss from the surface. All suspensions used contained TiO_2 nanoparticles with a nominal size of 20 nm and an average size of 26 nm.

The density profile variations included depositions with three distinct suspension formulations contributing to the final film. The three suspensions included a surfactant-less suspension, a suspension with PEG600, and finalized with a suspension with PEG20000. Additional variations had two regions: an initial layer from a surfactant-free suspension, then capped with either a PEG600 suspension or a PEG20000 suspension.

Immediately after assembly, the assembled DSSCs were tested under 1.5AM illumination, which delivered $100mW/cm^2$ to the surface of the photo-anode, inside an isolation

chamber. For each DSSC the short circuit current (I_{sc}), open circuit voltage (V_{oc}), and I-V curve were obtained while illuminated. From the I-V curve the maximum power point P_{max} was identified along with the associated current I_{MP} and voltage V_{MP}. The device Fill Factors were calculated according to Equation 1-1. Table 10 shows device measurements for DSSCs with uniform TiO_2 layers deposited via inkjet printing of varied suspensions.

Table 10: DSSC results with inkjet printed, uniform composition TiO_2 layers of different thicknesses. Note: a 4 micron thick deposition of a PEG20000 containing suspension could not be produced that maintained full area adhesion after sintering.

	1.46µm ± 0.14			4.35µm ± 0.21		
Surfactant	Isc (mA)	Voc (V)	Fill Factor	Isc (mA)	Voc (V)	Fill Factor
None	**0.342**	**0.30**	**0.47**	**0.680**	**0.36**	**0.49**
PEG600	**0.387**	**0.37**	**0.52**	**0.731**	**0.39**	**0.54**
PEG20000	**0.443**	**0.36**	**0.48**	**--**	**--**	**--**

The layer thicknesses of the TiO_2 films were built up over the course of a number of inkjet printing passes. Measurements of the film thickness were obtained using an AFM analysis of the height differential between various surface points and the substrate. The device Fill Factors and the short-circuit current showed an improved with the incorporation of PEG as a pore-forming agent.

For the non-uniform layers, a surfactant free suspension was deposited as the initial layer in the TiO_2 film. This was then covered by suspensions containing PEG. Three variations were produced, one which three layers and two other with two layers. Table 11 shows results for DSSCs with non-uniform TiO_2 layers.

Table 11: DSSC device performance with printed TiO_2 layers having varied deposition profiles. The approximate thickness of each film was 4 microns.

	Surfactant Profile	Isc (mA)	Voc (V)	Fill Factor
1	2µm None/ 1µm PEG600/ 1µm PEG20000	1.14	0.48	0.56
2	2µm None/ 2µm PEG600	0.87	0.41	0.51
3	3µm None/ 1µm PEG20000	1.10	0.43	0.53

Variations 1 and 3, with a top layer formed from a PEG20000 suspension, showed a notable increase over the PEG600. This would be expected given the increased surface area afforded by the increase in surface area provided by the more porous surface. The Fill Factor of the tri-layer film did show an improvement over the double layers as well as an increases in current and open-circuit voltage.

I-V curves of DSSCs corresponding to the density profile variations listed in Table 10 are shown in Figure 29.

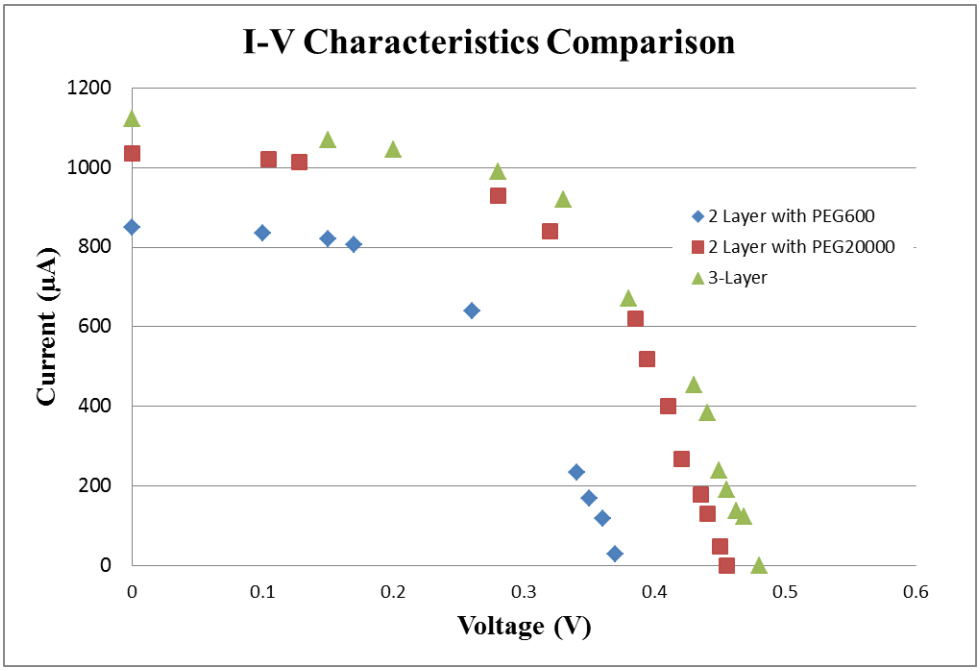

Figure 29: I-V curves for DSSCs with inkjet printed TiO_2 films of varied composition. The curves correspond to the density variations listed in Table 10.

The curves for the two cells with a top level formed from a PEG20000 suspension deposition are similar but the 3-section cell had a slightly higher maximum power point as well as a higher short-circuit current and open-circuit voltage. The shapes of the I-V curves do indicate the presence of significant series resistance accounting for the lower calculated Fill Factors. Changing the catalyst used in the assembled DSSCs from carbon to a more effective

catalyst such as platinum would be one avenue to improve the overall cell performance. Another option would a change from the ITO coated substrate to an FTO substrate.

The tri-layer TiO_2 films showed an average improvement in the Fill Factor of 8% versus single layers and 6% versus double layers. This was primarily attributed to an assumed increase in the conductivity through the layer and a corresponding decrease in series resistance. Short-circuit currents in tri-layer films increased an average of 35% over single layers and 13% over double layers. The major source of improvement in the current was associated, as was expected, with the TiO_2 films with a top layer formed with a PEG20000 surfactant to increase the surface pore volume.

Table 12 provides results from DSSCs with spin-coated TiO_2 films as part of the photo-anodes. The films had a uniform composition.

Table 12: DSSC results with spin-coated, uniform composition TiO_2 layers of different thicknesses.

	1.78µm ± 0.11			4.08µm ± 0.19		
Surfactant	**Isc (mA)**	**Voc (V)**	**Fill Factor**	**Isc (mA)**	**Voc (V)**	**Fill Factor**
None	0.327	0.43	0.49	0.512	0.40	0.46
PEG600	0.348	0.34	0.42	0.758	0.48	0.51
PEG20000	0.437	0.14	0.21	--	--	--

The spin-coated suspensions produced lower currents and Fill Factors compared to the corresponding inkjet printed DSSCs. Some this difference can be attributed to slightly thinner total film thicknesses. The lower Fill Factors may be a consequence of less mixing of deposited suspensions in the interface region.

The spin coating of suspensions with PEG20000 proved difficult to achieve, the resulting layers usually showed poor adhesion to the substrate. This possibly indicated that a reduction in the PEG concentration was in order. Table 13 gives results from the use of TiO_2 films with varied density profiles.

Table 13: DSSC device performance with spin-coated TiO_2 layers having varied deposition profiles. The approximated thickness of each film was 4 microns.

	Surfactant Profile	Isc (mA)	Voc (V)	Fill Factor
1	2µm None/ 1µm PEG600/ 1µm PEG20000	0.97	0.39	0.55
2	2µm None/ 2µm PEG600	0.82	0.35	0.47
3	3µm None/ 1µm PEG20000	0.91	0.37	0.51

The tri-layer spin-coated DSSCs did provide a close match to inkjet printing in terms of Fill Factor but produced lower currents and voltages.

The inkjet printed samples generally outperformed the similar spin-coated samples. The layer thickness should also account for a portion of the performance difference. The area of the deposited films was kept constant for each of the depositions and the time spent immersed in the dye solution was equal for all samples.

The best performing DSSCs TiO_2 films with PEG20000 suspensions deposited at the top and with denser layers underneath. A few other trends are seen in the measurements including an increase in short circuit current and fill factor with increased thickness, an increase in short circuit current with films have PEG20000 suspension on the top level of the surface, and an increase in open circuit voltage and fill factor with the use of the surfactant free suspensions deposited as a base layer.

6 Discussion

The research project explored the effect on DSSC device performance when the photo-anode had a TiO_2 film with a graded density profile—with a higher density on the bottom and a highly porous top surface. For the deposition of the TiO_2 films with varied density, the use of inkjet printing was explored as an alternative to the traditional method of spin-coating. In this section, the major results are discussed and potential avenues of future refinement identified.

6.1 Suspension Preparation

The preparation of a printable suspension was a basic requirement prior to using an inkjet printer as a means of deposition. In particular, the suspension had to be free of particle masses beyond the limit imposed by the size of the printhead nozzles. Further, the suspension had to be stable against the formation of large masses after insertion into the printing system. The presence of large particle masses led directly to increased rates of sedimentation for stored suspension and caused blockages in the printing system.

As TiO_2 is not a soluble material, the suspension formulations that were developed ultimately required the use of a milling apparatus and filtering in order to eliminate large particles and aggregates. To achieve reliable dispersion of the particles, a pH adjusted suspension solution with ethanol as a co-solvent was used. The addition of PEG as a surfactant was observed to help increase the particle dispersion.

An acidic suspension pH is often not desirable, depending on the deposition method. Epson printer ink generally has a basic pH and the printing system is designed accordingly. A major benefit to using a basic pH is the reduction of corrosion that occurs in the printing system. TiO_2 particles themselves produce an acidic pH when mixed into a neutral fluid, a fact which must be accounted if an attempt is made to balance the pH of the suspension to a neutral or basic

level. As particle dispersion is most readily promoted by charge screening by ions, a neutral suspension pH requires the use of non-ionic stabilizers. It is possible that PEG, in suitable concentrations, could adequately provide a uniform dispersion and was assumed to partially have done so for the suspensions developed in this work. A further study would be required to determine the PEG concentration levels needed to achieve dispersion stability for a neutral solution and what types of pH adjustments would be needed to neutralize the acidifying effect of the TiO_2 particles.

6.2 Layer Density Variations

A twofold approach to producing density variations in deposited layers was attempted: to use surfactants of different molecular weights to vary the pore volume and to vary the sizes of the TiO_2 particles through the attrition grinding of initially micron-sized particles.

Using different surfactants or no surfactant at all was observed to directly affect the morphology of deposited surfaces. The most reliable measure of the effect was the surface roughness; with increased surfactant weight, the roughness increased. SEM images showed qualitatively that the surfactant content increased the pore content of deposited films and consequently decreased the overall density at the surface level. Developing additional suspensions with PEGs of molecular weights between 600 and 20000 g/mol would allow for additional grading of the TiO_2 film simply on the basis of varying pore volume.

The approach of reducing micron-sized particles to obtain a distribution of smaller particles within the printable range through the use of attrition milling, proved to be ineffective. The intent was to vary the film density through successive depositions of suspensions having decreasing average particle sizes. The end results of the grinding were nanoparticles with diameters of less than 50nm or else the particles were not reduced to printable sizes. Filtering did

offer some benefit towards reaching a printable suspension. But the filtering removed a significant amount of the particles and the approach was deemed an inefficient use of material.

Other possibilities could be explored with the goal of varying density through particle size variations such as synthesizing particles with the desired size. Another possibility is using more advanced filtration techniques to more effectively separate particles within a given size range.

6.3 DSSC Device Performance

Several trends in device performance measurements were observed for the different TiO_2 film variations. These included a higher short-circuit current for devices when a suspension containing PEG20000 was deposited on the top level of the TiO_2 film. Devices having a substrate level deposition of the surfactant free suspension, acting as a dense base layer, saw an improvement in the open circuit voltage. Thickening the layers with additional printing passes or spin-coatings also improved the open circuit voltage and the fill factor.

DSSCs with printed TiO_2 layers consistently outperformed similar cells with spun-on TiO_2 layers but a direct comparison was not possible. While the same materials were used for both deposition methods, the film thicknesses were not equal and TiO_2/surfactant concentrations were higher for the spin-on formulations. For the films formed with a varied density profile, the three-fold film preformed the best of all of the variations tested. This was the case for both the printed and spun layers.

Additional testing could serve to establish an optimal ratio of the film's composition. The results suggested that a relatively thick high density base covered by thin coatings of progressively lower density could give the best performance. Device fill factors and overall device performance appeared limited by the choice and quality of the catalyst applied to the

counter-electrode; with a more effective catalyst, such as platinum, the device performance could possibly be more readily distinguishable across different sample variations. This would allow for a more effective determination of the optimal TiO_2 composition and density profile.

6.4 Printing System Assessment

The adaptation of a commercial inkjet printer for the deposition of TiO_2 suspensions can only be successful if the suspension falls within the printable range of the printing system. The nozzle size of the Epson Artisan 730, at 20 microns, effectively limits the maximum size of particles dispersed in suspension to the submicron scale in order to avoid the rapid development of blockages. A larger nozzle size would accommodate larger masses present in the suspension. Some nozzle blockages are difficult or impossible to dislodge once in place; a permanent printhead in the printing system is not ideal for this reason. Having a replaceable printhead also provides flexibility in ensuring that residue from suspensions does not contaminate subsequent printings when a new or different suspension is used.

As metal oxide nanoparticles have the tendency to aggregate in aqueous solutions, TiO_2 suspensions must have consistent dispersion stability in order to reliably print. Provided the suspensions contain only nanoparticles with good dispersion stability, the system can print effectively.

The particular printer used was not the most efficient for testing purposes in terms of preparation time or material usage: long feed lines required flushing between suspension variations and then had to be re-filled in order to begin printing. Short feed lines or a direct attachment of the ink reservoir to the printhead would be a significantly better arrangement.

The 6 ink lines in the Epson 730 did provide an advantage for the printing of films with multiple layers of varied compositions. Specific lines can be dedicated for specific suspension variations, allowing for immediate depositions in sequence.

Suspension formulations developed for this project should be further refined to achieve a greater match to the specific design of the printing system. This would include an analysis of the viscosity, surface tension, and density of the original inks and matching the suspension properties to fit the measured values as closely as possible. A suspension with matched fluid characteristics should provide a greater consistency in printing with respect to jetted droplet size. An increase in consistency should aid in the deposition of more uniform layers.

7 Conclusion

Based on the characterized surface properties of deposited TiO_2 films and the corresponding effects on DSSC performance, a graded density profile in the TiO_2 film was associated with a positive increase in performance over devices with a uniform film. Increasing the number of steps in the density profile also correlated with performance improvement. DSSCs with printed TiO_2 films having three density layers showed an average improvement in the Fill Factor of 8% versus single layers and 6% versus double layers. Short-circuit currents in tri-layer films increased an average of 35% over single layers and 13% over double layers.

For achieving deposited layers with varied density, the use of PEG as a surfactant in suspension formulations proved successful whereas the attrition grinding of large particles did not. PEGs of different molecular weights produced surface morphologies with discernible differences compared to each other and to surfaces formed from suspensions without surfactants. Two PEGs with molecular weights of 600g/mol and 20000g/mol were used. Developing additional suspensions with intermediate molecular weights would provide a means to further grade the density profile of deposited films.

Suitable suspensions were formed using TiO_2 nano-particle powder with a nominal particle size of 20nm, pH adjusted water, ethanol, and PEG. The preparation procedures produced suspensions which showed good stability over an extended storage period. As part of the suspension preparation, a milling apparatus proved necessary to reduce the presence of large aggregates and avoid blockages in an inkjet printing system. The inkjet printer selected was able to deposit suspensions when filtering steps were employed and provided the suspensions were used within two days of preparation. Inkjet printed layers were also associated with better performance than spin-coated layers.

The use of inkjet printing as a deposition method for the deposition of DSSC photo-anodes shows a great deal of potential. There are several options for its use, ranging from the deposition of the entire film or as a means of applying a top coating to a thicker base layer deposited by other means.

Appendix A: Photovoltaic Technologies

A.0 Introduction

Consistent and reliable access to adequate energy supplies is a key necessity for the stability of modern technological societies. The search for cost effective, abundant, and environmentally sustainable energy sources that can serve as alternatives to fossil fuels has motivated research into a number of promising technologies. These possibilities have included wind, hydroelectric, tidal, nuclear, geothermal, and solar. For each of these, particular attention has been paid to the technology's level of long-term sustainability, environmental impact, and accessibility.

Of the alternative energy options, solar energy presents itself as the most attractive in terms of sustainability: light produced from the fusion of the sun's supply of hydrogen will continue for billions of years; in terms of environmental impact: solar-powered energy conversion systems can be easily produced using non-toxic materials and processes, and a solar power installation's stationary nature poses minimal risk to wildlife; in terms of accessibility: sunlight is available in varying degrees and lengths of time to every part of the earth's surface. Solar energy is also the most plentiful. If one hour of the sunlight reaching the planet's surface could be completely captured, it would be sufficient to meet global energy needs for an entire year [32]. Alternatively, if 0.1% of the earth were covered by solar cells with at least 10% energy conversion efficiency, all the global energy needs could be met [33].

Solar-powered electrical generating systems convert solar energy directly into electricity through the photovoltaic (PV) effect. The photovoltaic effect is a property exhibited by certain materials and involves the release of atomically or molecularly bonded electrons through absorption of energy from incident photons. The effect occurs when incident photons have

energy sufficient to overcome the bandgap of the material—where the bandgap refers to the difference in energy of the Highest occupied molecular orbital (HOMO) and the Lowest unoccupied molecular orbital (LUMO). Effectively, the photons excite electrons out of valance bands, which are the highest occupied orbitals, and into conduction bands, the lowest unoccupied orbitals, creating electron-hole pairs in the material. Released electrons are known as photoelectrons and resulting currents as photocurrents. Solar cells are invariably made using semiconductor materials and so are sometimes referred to as photovoltaic cells.

One of the major ongoing research tasks associated with solar cells is to achieve as high an energy conversion efficiency as possible while keeping material and processing costs as low as possible. A cell's efficiency is determined by a number of factors but chief among them are how much of the incident spectrum can generate photoelectrons and the ease with which the photoelectrons can be passed out of the material and into an attached circuit.

A.1 Solar Cell Technologies

Solar cell technologies have progressed through a number of generations. The first generation cells used the traditional Group IV semiconductors Silicon (Si) and Germanium (Ge) or Group III-V combinations such as Gallium arsenide (GaAs). Second generation solar cells are based on thin-film devices which are much easier and cheaper to manufacture.

Amorphous Silicon (a-Si), Cadmium Telluride (CdTe), and Copper indium gallium selenide (CIGS) are the most common photovoltaics used in thin-film cells. Both the first and second generations relied exclusively on single junction devices [1]. In a single junction device, the conversion between solar energy to electrical takes place in the depletion region between a p-type (electron acceptor) and n-type (electron donor) material. Any electron-hole pairs produced by solar excitation in the depletion region are separated by a built-in electric field.

Third generation cells use multi-junction devices, each junction captures a different portion of the electromagnetic spectrum, increasing the overall cell efficiency. Next generation devices incorporate nano-technology to enhance spectral response, reduce material costs, and relive material purity requirements. What follows is a brief summation of examples from each the three initial generations of solar cells.

A.1.1 Silicon

Silicon can take a variety of forms in solar cells including mono- and poly-crystalline, amorphous, and thin-film. Crystalline silicon (c-Si), in both poly and mono forms, has held a dominant lead in terms of commercial market share over other PV technologies for a number of years. In 2010, c-Si accounted for 83% of total cell production with the majority of that portion attributed to polycrystalline silicon cells [34]. Following a significant drop in crystalline silicon cell costs in 2011, the market share of c-Si is projected to increase over the next several years with high efficiency single crystalline silicon becoming more prevalent within that category [33].

A number of factors have favored silicon as a solar cell material. Silicon is abundant, non-toxic, and highly stable when properly sealed. Commercial silicon solar panels have impressive long-term performance: providing up to 80% of the rated power output for 25 to 30 years after initial installation. Conversion efficiencies of silicon solar cells depend on the crystalline form and ranges from near 25% (c-Si) to 10.1% for amorphous-Si [35]. In the case of silicon, the theoretical maximum efficiency has been shown to be 30%; the maximum possible efficiency for any single-junction cell has been determined to be 33% [36].

A.1.2 Thin-Film

Thin-film systems using cadmium telluride (CdTe) modules have the second highest market share after silicon cells with 6% of the PV market [34]. Owing to lower solar energy

conversion efficiencies, a thin-film installation can require up to 40% larger area compared to c-Si in order to achieve equal electrical energy outputs. However, thin-film installations can reach specific output energies at a lower cost (0.84 USD versus 1.1 USD for mono c-Si) due to a less expensive manufacturing process [23]. A major drawback to thin film cells are the toxicity of the materials used, especially cadmium, and also the relatively low abundance of the materials [37]. The manufacturing of thin-film cells can be done at a large scale on flexible substrates in an automated production process. This is an advantage over crystalline silicon PV technologies which, at the cell level, can only be produced with a much smaller surface area.

A.1.3 Multi-Junction

Multi-junction cells have the highest recorded solar energy conversion efficiencies of any PV technology. State of the art cells have verified efficiencies greater than 43%. The concept behind multi-junction solar cells is to provide a number of junctions with different band gap energies to capture a wider energy range of incident photons with as little loss as possible. In all multi-junction cells, the junctions are stacked with the highest band gap junction at the top and each successive junction having a lower band gap. High energy photons are captured first and the lower energy photons are progressively captured at lower junctions.

Ideally, the junctions would cover as wide a range of band gaps as possible with a small difference between adjacent junctions. Theoretical models put a maximum limit of 86.8% for conversion efficiency in the case of an infinite number of junctions, each with a different band gap. Multi-junction cells with 2, 3, and 4 junctions have been calculated by Marti and Araujo [38] to have maximum one-sun efficiencies of 32.5, 44.3, and 53.6 respectively.

Appendix B: DSSC Operating Principles and Research Trends

This appendix provides additional information on the principles that govern the photo-current generation in a DSSC. Also offered is an overview on some of the significant material and device research trends being investigated by DSSC research groups.

Even though standard dye sensitized solar cells have a reasonably simple structure, their ability to convert solar energy into electrical currents is governed by a number of complex interface reactions. The reaction with the lowest overall efficiency effectively determines the overall device efficiency. Efforts to improve DSSCs to a performance level competitive with that of other photovoltaic technologies have focused on several fundamental areas involving material selection and device fabrication. To achieve general acceptance as a viable alternative to silicon solar cells, DSSCs must achieve higher efficiencies using sustainable, nontoxic materials and must also exhibit long-term stability in outdoor usage.

Investigations into new materials aim to reduce costs and improve performance. Research at the device level considers issues of long-term stability, device structure, and scalability among others.

B.1 DSSC Device Operating Principles

For the photo-current induced in an illuminated DSSC to complete an electrical circuit, electrons must travel along a path that involves several distinct stages, each requiring specific reactions in order to advance the current flow.

Photons enter into the cell through the TCO of the photo-electrode and pass through the TiO_2 semiconductor layer; TiO_2 is highly transparent for photons with wavelengths greater than ultra-violet. Absorption of a photon with a sufficient energy can elevate an electron in a dye molecule from the Highest occupied molecular orbital (HOMO) energy level to the Lowest

unoccupied molecular orbital (LUMO) energy level. This electron excitation allows for the potential injection of the electron into the conduction band of the TiO_2, which is at a lower energy level than the dye's LUMO.

As the highest energy level of electrons in iodide is higher than the dye's HOMO, an electron transfer and re-oxidation of the dye is facilitated. The open circuit voltage of the DSSC is determined by the difference between the TiO_2 Fermi level and the potential of the redox couple [39].

Figure B-1 shows the energy level transitions that occur in a standard DSSS.

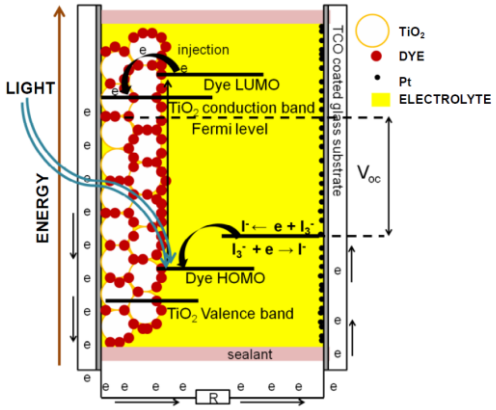

Figure B-1: Schematic of a DSSC showing the energy level transitions for reactions involved in the device operation [39].

A number of undesirable electron paths resulting from defects, back reactions, and recombinations contribute to decreases in overall device efficiencies by interfering with individual steps in the charge transfer cycle. Back reactions occur when electrons from the TiO_2 film are directly transferred into the electrolyte without reaching the electrode. Recombinations are a particular concern at the dye-semiconductor interface where newly induced photoelectrons are immediately reabsorbed by the dye rather than injected into the semiconductor layer.

B.1.1 Photosensitizer Excitation

Photosensitizing molecules are the distinctive feature of DSSCs and are required as the band gap of the semiconductor is too large for effective photocurrent generation. For most sensitizer molecules used in DSSCs, the center of the absorption occurs for photons near 550nm and extends over the visible range of light.

After absorption, the sensitizer reaches an excited state and releases an electron. A typical dye molecule can stay in an excited state for several nanoseconds before dropping back to the ground state. Once in the ground state, the now oxidized dye molecule must reacquire an electron to maintain charge balance.

B.1.2 Photoelectron Injection

A dye that is adsorbed onto a metal-oxide nanoparticle will inject a photoelectron into that particle extremely fast, on the order of femtoseconds to picoseconds depending on the excited state of the dye. Ideally, the injection rate should be 100 times greater than the decay rate of the oxidized sensitizer. Also, the energy level of the sensitizer must be 0.2 to 0.3V above the conduction band edge of the oxide for electron transfer [1]. This potential represents the minimum driving force required to push the photoelectrons into the conduction band of the semiconductor.

B.1.3 Semiconductor Transfer

A nano-structured metal-oxide layer in a DSSC has particle sizes that cannot generate a macroscopic electric field. Thus, charge transport through the oxide occurs through a kinematic diffusion process, the exact nature of which is still debated [40]. Electron diffusion imposes a requirement that the thickness of the layer be less than the diffusion length of the electron. A possible path for the free electrons in the oxide is to be recombined with acceptors in the

electrolyte. For efficient charge extraction from the oxide layer, the overall electron lifetime needs to be greater than 20μs for a 10 micron thick oxide layer [6].

B.1.4 Redox Couple Reduction

The electrolyte in a DSSC acts as a hole conduction medium that shifts the hole generated by the photo-excitation of the dye to the counter-electrode. To maintain the hole current in the electrolyte, the holes must be filled with electrons from the counter-electrode. Since the hole transfer occurs through a diffusion process, the reduction of the redox couple has to occur at a very fast rate compared to the recombination rate of electrons at the interface between the oxide layer and the electrolyte. To speed the reduction process, a catalyzing agent is required.

B.1.5 Sensitizer Regeneration

Regeneration of the sensitizer—a donation of an electron to the sensitizer from the electrolyte—occurs in the nanosecond range with iodide/tri-iodide electrolytes. The lifetime of an oxidized dye molecule is taken into account when designing DSSCs for extended useful lifetimes (>20 years). Cell performance decreases with age as oxidized dye molecules decay from not being regenerated fast enough. Ruthenium dye complexes are well suited for extended device operation as their lifetime in an oxidized state is typically greater than 100 seconds [41]. Coupled with iodide/tri-iodide electrolytes, few losses due to dye decay occur over an extended period of time.

DSSC materials are selected to maximize the efficiencies and speeds of each of the necessary reactions. That key reactions take place at dramatically different rates is what enables a DSSC to work. In particular, the lifetime of a typical dye molecule in an excited state is in the nanosecond range but the photo-electron injection into the semiconductor occurs on the order of

a femtosecond. Thus the dye can exist in an excited state significantly longer than it takes to unload the electron into the semiconductor. Most important of all reaction rates is that of the back transfer of electrons into the dye which occurs in the micro- to milli-second range. This slow rate of recombination enables the charge separation to take place, without which a photocurrent cannot be established.

B.2 DSSC Material Research Trends

There are presently two streams of DSSC material research: optimization of materials and processes for large area device manufacture at competitive costs; exploration of new materials, structures and device fabrication procedures to achieve higher energy conversion efficiencies. A major remaining concern is the long term stability of assembled cells, particularly when using liquid electrolytes. Long-term stability requires attention to another critical component of a practical DSSC, that of an encapsulating sealant to prevent the ingress of H_2O and the evaporation of the electrolyte.

What follows in this section is a brief discussion of some of the major ongoing research topics for the major elements of DSSCs.

B.2.1 Cell Substrate and Counter-Electrode Catalyst

A DSSC has two electrodes: the cathode, known as the counter-electrode, where electrons return from the external circuit and the anode, called the photo-anode or photo-electrode, where electrons generated through photo-excitation pass out of the cell. The substrates of the electrodes may or may not be the same material; the only real requirement is for the substrate on the photo-electrode side to have a high degree of transparency for that is the direction of illumination.

Transparent conducting oxides (TCO) in the form of a thin film conducting oxide coating on a clear glass substrate are commonly used for both of the electrodes in a DSSC. The TCO needs to provide a low resistance path for the generated photocurrent to and from the external circuit. The two most widely used oxides are Fluorine-doped tin dioxide (FTO) and Indium tin oxide (ITO). FTO is generally favored over ITO, despite having a lower conductivity, because it has better chemical and temperature stability. Glass as a base substrate for the conducting oxides is attractive due to its low cost and high optical transparency.

FTO and ITO coated substrates do suffer from low carrier mobility and work has been done on finding a high mobility alternative. One candidate is titanium doped indium oxide (ITiO), which possesses higher carrier mobility and also has a higher optical transmission. Comparison tests between FTO and ITO have shown a 4-fold increase in mobility, a reduction in layer resistivity and sheet resistance, and a 60% higher transmission of light in the wavelength range 700-1400nm [42].

Another area of research is in the use of flexible substrates which are appealing by providing the option for installation on irregular surfaces and also for a greater ease in the transport of solar modules and panels. A number of different substrates have been investigated such as ITO-coated polymers, titanium, and stainless steel [37].

The purpose of the catalyst is to speed the reduction of the redox electrolyte by completing the charge transfer from the TCO to the electrolyte. For the iodide/tri-iodide redox couple this entails the reduction of the tri-iodide to return it to an iodide form. The catalyst selected for activation of the counter-electrode must meet several basic requirements in order for the DSSC to function properly. The critical requirements are that the catalysts have a low charge

transfer resistance, possess a high chemical stability when exposed to the electrolyte, and generate a high level of catalytic activity at the electrolyte/electrode interface.

Platinum is the most common catalyst used because it fulfills these requirements very well. Platinum is, however, quite expensive and when used with a FTO coated glass substrate, the counter electrode can account for up to 60% of the total cell cost [43].

Carbon in various forms and conducting polymers have been employed as a lower cost, chemically stable catalysts and, while able to work, the electro-catalytic activity is lower than platinum and results in lower overall cell efficiencies [39]. Carbon black and stainless steel have been used for a catalyst, ultimately yielding a DSSC with 8.86% conversion efficiency [44]. One very simple way to deposit a carbon catalytic layer on an ITO or FTO glass substrate is to pass the glass through a candle flame repeatedly until a dark, uniform layer of soot develops.

B.2.2 Semiconductor Layer

Material choices, processing methodologies, and the specific nature of the nano-structuring of the wide bandgap semiconductor are among the important factors that determine the overall performance of a DSSC. A key requirement of the semiconductor is that it possesses a high resistance to photocorrosion, a property shared by a number of metal oxides such as Titanium dioxide (TiO_2) and Zinc peroxide (ZnO_2), but not by traditional semiconductors such as silicon.

To date, a wide variety of metal oxides have been investigated but TiO_2 DSSCs have yielded the highest recorded efficiencies. Preparation of the TiO_2 nano-particles themselves involves the hydrolysis of a titanium precursor, thermal growth, and crystallization. By varying the exact technique used, the nature of the nano-structures that form can be adjusted. This allows for the creation of nano-wires, rods, tubes, bowls, sheets, and spherical particles of various sizes.

Modern implementations of DSSC rely on the dramatic increase in the surface area of the semiconductor layer provided by the use of the nanostructured metal oxides, which allows for an increased number of dye molecule attachment points. The large surface area due to the small particle size has the drawback of decreasing the electron transport through the semiconductor layer.

To control the final morphology of a TiO_2 layer and to help prevent nanoparticle aggregation, surfactants that act as chemical dispersants are used. A common dispersing agent is Polyethylene glycol (PEG) which is available in a wide range of molecular weights. PEG has been observed to help prevent aggregations of nanoparticles and to produce pores in the 50 to 200nm range [45]. Another frequently used chemical in DSSCs is acetic acid which acts as a solvent for TiO_2 in solution [46]. A sintering at 450°C for 15 minutes of a deposited TiO_2 layer is the usual procedure for forming the nanostructured layer; the high temperature drives out the solvents producing a highly porous layer which is then soaked in a sensitizer solution.

B.2.3 Photo-sensitive Dye

Photosensitizers in DSSCs are dye molecules that absorb photons of wavelengths that correspond to the bandgap of the dye. This causes the dye to become oxidized and allows an electron to be injected into the conduction band of the TiO_2 layer.

For a dye to be a viable choice for use in a DSSC, it must possess several basic characteristics. These include a strong absorption of light in the visible region of the spectra, strong adsorption onto the surface of the semiconductor layer, and fast injection of photoelectrons into the semiconductor [47]. In addition, the dye must have a high degree of chemical stability when exposed to the solvents in the electrolyte solution. Thousands of dye

formulations have been tested to date, ranging from simple and inexpensive to finely crafted molecules that are very costly.

Ruthenium (Ru) based compounds were among the first dye molecules studied and DSSCs incorporating them still produce among the most efficient cells. One of the well-known Ru-complexes developed by Gratzel and coworkers still in wide use is N-719, a dye molecule with good performance in two key areas: light absorption and charge transfer. The N-719 dye absorbs photons with a wavelength between 400nm to 900nm [40]. Other ruthenium based dyes, such as the N-749 or black dye, have since been chemically engineered with an extended spectral response into the near-IR region [1]. Ruthenium is not an abundant metal; the dyes that use Ru-complexes are expensive and DSSC designs that incorporate them do not represent environmentally sustainable solutions.

Naturally occurring dyes have been studied as an alternative to chemically engineered dyes but exhibit lower light collection capability and produce DSSCs with low efficiencies, typically less than 1% [48]. Natural dyes do offer several advantages: a variety of inexpensive and plentiful sources are available; dye solutions are simple to prepare with common materials and minimal equipment and natural dyes are adsorbed onto the semiconductor layer rapidly.

B.2.4 Electrolytes and Hole Transfer Materials

The most successful liquid electrolyte is the iodide-triiodide (I^-/I_3^-) redox couple due to long electron lifetimes, fast electron transfer into dye molecules, and fast regeneration at the counter-electrode. Iodide electrolytes have been verified to have long term chemical stability [49]. The choice and characteristics of the solvent for the redox couple has a significant impact on the overall device performance. A commonly used solvent is acetonitrile, a medium-polarity organic nitrile, which displays good dye regeneration while also reducing back electron transfer

by passivating the semiconductor surface, effectively isolating the metal-oxide from ion contact [41].

The ions in the I^-/I_3^- redox couple are highly polar molecules and finding a suitable long term sealant for DSSCs has been an ongoing challenge. Several commercial hot-melt polymer sealants, notably Surlyn and Bynel, have been used [50]; these sealants exhibit instability under varying temperatures and are not especially suitable for large scale manufacturing of DSSCs. Leakage of the electrolyte resulting from a sealant failure is a major cause for reduced DSSC lifetimes. One option to reduce electrolyte leakage and evaporation is to increase the viscosity of the electrolyte through a polymerization process or the addition of SiO_2 particles. The result is referred to as a quasi-solid electrolyte which exhibit good stability but lower efficiencies [51].

Replacing the liquid electrolytes with a solid-state Hole-transport material (HTM) is widely considered a necessity for large scale and long-term use of DSSCs. One example of a solid state HTM is a solution containing spirofluorine and additives. This solution is applied to the surface of a TiO_2 layer, allowed to permeate for 60 seconds, and then spin at 2000 rpm for 30 seconds which forms a solidified heterojunction [52]. Back contacts can be added through the thermal evaporation of a suitable contact metal.

B.2.5 Next-Generation DSSCs

As with other photovoltaic technologies, one of the major research goals is to extend the absorbable spectrum as far as possible. There are several ways to achieve this goal with DSSCs including tandem cells which have a stacked arrangement of a number of different photosensitizers. This approach suffers from the incomplete transparency of the cell components which reduce the number of photons reaching lower levels of sensitizers.

A second option is to incorporate combinations of co-sensitizers into the cell to extend the spectral range. This could include adding additional dyes with lower bandgaps to extend the minimum photon energy that can be absorbed. Alternatively, the use of dyes could be eliminated entirely and replaced with quantum dots, which offer the possibility of fine-tuning the spectral range by varying the size and material composition of the dots [53]. This class of solar cell is usually differentiated from DSSCs and known as Quantum dot sensitized solar cells (QDSC). Solid state QDSCs have exhibited energy conversion efficiencies between 5% and 6% [54].

B.2.6 State of the Art DSSC

The DSSC with the highest recorded solar energy conversion efficiency was reported in 2013 at 15% with a fill factor of 0.73 [5]. This cell used a HTM in place of a liquid electrolyte and a perovskite sensitizer. In other respects, the state of the art cell is similar to the standard cell in that FTO slides were used as a substrate and TiO_2 nanoparticles were used as the semiconductor base for the photo-sensitizer. In place of platinum, gold was used as a catalyzing agent. For the TiO_2 layer, the researchers first deposited by spray pyrolysis a thin and compact layer of TiO_2 particles. This was then covered by a thicker TiO_2 layer that was deposited by spin-coating.

B.3 Key Challenges for DSSCs

Several key barriers remain to a wide spread use of DSSCs as a prevailing photovoltaic technology. These include issues of low efficiency compared to traditional semiconductor cells, problems with scaling the devices to the module level, and long-term stability issues.

B.3.1 Efficiency

The highest DSSC efficiencies that have been achieved are still much lower than those of the crystalline silicon solar cells. Improvements in cell efficiency can be achieved in a number of ways but all involve either increasing the short circuit current or the open circuit potential. Photo-currents can be increased by extending the absorption range of the sensitizing agent as far as possible while minimizing recombination reactions. Open circuit voltages can be increased by reducing the energy loss in the sensitizer regeneration by the electrolyte.

B.3.2 Scalability

Transitioning DSSCs to the module and panel level has proven difficult to achieve without experiencing significant losses in device performance. A major performance issue with large scale dye sensitized modules centers on the accumulation of energy losses due to series resistance of individual layers. The primary source for the series resistance is the substrate which requires the use of conductive fingers with series connected cells. In the design of the conductive pathways, a balance must be struck between resistance loss and active area loss [55].

The up-scaling of DSSCs necessarily involves the connection of individual cells into modules to produce adequate output voltages. There are several structural schemes for the interconnection of cells into modules including serial, parallel, and monolithic arrangements [56]. Another major problem with up-scaling standard DSSCs with liquid electrolytes involves the need to ensure long-term sealing and protection of the liquid. Elimination of the liquid electrolytes in favor of quasi-solid and solid-state HTMs will greatly simplify module manufacturing processes and necessitate less stringent sealing requirements.

B.3.3 Stability

Of particular concern for the long-term stability of a cell are the effects of prolonged exposure to sunlight, temperature variations and extremes, and structural integrity when installed outdoors.

The stability of many individual materials is well established under laboratory conditions. For example, ruthenium-based dyes have been shown to have strong molecular stability and are anticipated to have a usable life of 20 years or more [50]. Liquid electrolytes, including iodide/tri-iodide complexes, have shown a marked vulnerability to UV light and require filtering to protect against degradation [57]. Solvent free electrolytes have been shown to reduce deterioration by 80% compared to electrolytes with solvents [58]. The TiO_2 layer in standard cells has been observed to accumulate electrons under continuous illumination and this effect is theorized to be responsible for an increase in the rate of back electron transfer in aged cells [59]. The prolonged integrity of cell sealants is the primary determinant of cell lifetime. The commonly used seals are thermoplastics or foils and allow diffusion of electrolyte solvents at elevated temperature [50].

Appendix C: TiO_2 Deposition Techniques

Metal oxide semiconductors have garnered extensive study in recent years and their use has found application in a wide range of fields, devices, and consumer products [33]. One of the more commonly encountered metal oxides is Titanium dioxide (TiO_2), a wide bandgap semiconductor. The low cost, non-toxicity, and biocompatibility of TiO_2 have prompted common usage as a key component in pigment based inks and paint as well as sun screens and toothpaste [60].

Some applications, such as in DSSCs, require the formation of a thin layer of TiO_2 on a suitable substrate. The methods that have been utilized to produce the requisite layers fall into three main groups: physical vapor deposition including evaporation, sputtering, electron-beam epitaxy, etc.; chemical vapor deposition; and wet-chemical processing including spin-coating, dip-coating, screen-printing, and inkjet printing among others [11-14, 60].

C.1 Common Deposition Techniques

The various processes used for TiO_2 film depositions intend to form uniform and reproducible layers. The actual method used is often dictated by the available processing equipment. TiO_2 films can be easily processed with simple manual methods that do not usually achieve ideal results. Another traditional method for forming thin-films is that of dip-coating, a simple process that requires immersion of a substrate in a sol and with-drawing it at a constant speed. Spin-coating machines, a common piece of lab equipment found, are often employed for obtaining TiO_2 films of varying thicknesses. There still is a preference for automated depositions to achieve a higher degree of reproducibility and this has prompted the wide use of screen printing for TiO_2 films. Other options are available, but these four constitute the prevalent methods currently used.

C.1.1 Doctor-Blade

One of the most common TiO_2 deposition methods is a fully manual technique called doctor-blade [34]. A viscous TiO_2 is required and can be prepared using commercial nano-particles: equal parts by weight of TiO_2 powder and a DI water/acetic acid solution. The mixture is then ground in a mortar until a smooth and consistent paste is formed. A drop of surfactant is then added and slowly stirred into the paste. Tape applied to the substrate marks off the boundaries of the TiO_2 film and also provides a physical spacing between the substrate surface and the top of the film for the next step. After a quantity of the TiO_2 paste is placed on the substrate, a glass rod is used to 'blade' across the paste until a smooth and flat surface is obtained. Once the desired layer is produced, the tape is removed and the sample is sintered to drive out solvents.

Among the limitations of the doctor-blade method is the difficulty of obtaining reproducible results. The method also produces relatively thick TiO_2 layers in the range of 10 to 30 microns; thicker TiO_2 films have a greater chance for developing cracks or peeling off the substrate during sintering.

C.1.2 Dip-Coating

Morozova et al. prepared TiO_2 films using both dip-coating and inkjet printing using template sol-gels [60]. The dip-coating process involved the use of a laboratory dip-coater that immersed a substrate for 30 seconds and then withdrew it as a rate of 6 cm/min. The RMS surface roughness was measured to range between 0 and 5 nm, for the inkjet samples, 3 to 6 nm was measured.

In general, the formation of photo-anodes using the dip-coating method has been found to result in varying sensitivities as formed layers were quite different from each other. Additional calibration steps were found to be required, leading to additional expense and time [14].

C.1.3 Spin-Coating

Applying a quantity of TiO_2 to a substrate and spinning at a high rate causes centrifugal force to form a thin-film. The spin rate, time, and solution viscosity determines the thickness of the resulting film. Spin-coating also suffers from difficulty in generating reproducible layers which limits the viability of spin-coating as an option in the large-scale manufacture of DSSCs.

C.1.4 Screen Printing

In traditional screen printing, ink is transferred through a mesh according to a pattern defined by an ink-blocking stencil. Ink is applied to the screen with a squeegee and spread over the surface at a smooth and even rate. For the screen printing of TiO_2 the process is similar, with a TiO_2 solution in place of ink. Several factors have to be considered for the printing of a suitable layer including solution composition, mesh size, applied pressure, and speed [15]. The viscosity of the TiO_2 solution must be less than those required for doctor-blade and spin-coating technique. A rheological agent such as ethylcellulose is normally used to adjust the viscosity to a suitable level. Aggregation of nano-particles is also a concern and additives are required to maintain dispersion of the TiO_2 in the solution.

C.2 Inkjet Printing

A relatively novel approach for the deposition of TiO_2 films through the use of inkjet printing has begun to attract attention owing to its high level of control over the process and the possibility of direct patterning of layers [8, 9]. Specialty laboratory printers designed for printing

of solutions with a wide variety of fluid properties are available and have been used for TiO_2 depositions. This category of printer is, however, a significant investment, often costing tens of thousands of dollars. Commercial inkjet printers offer a potential low-cost solution provided they meet certain requirements and the solutions are within the printable range of the equipment.

Several major design variations exist for inkjet printers, variations that have been developed in response to the many diverse applications that printers have been tailored to over the past several decades [16]. There are two primary printer categorizations, continuous and Drop on demand (DOD), that are often used to differentiate commercial and industrial printing from consumer printing. The distinction is based mainly on whether ink is being jetted from the printer in a continuous stream or as individual droplets. The actual ink jetting is an action performed by the printhead of the unit and can be achieved through one of two methods: thermal or piezoelectric.

Both of these printhead types can be found in fixed or disposable variations. Generally, thermal printheads are designed to be regularly replaced whereas piezoelectric printheads, being significantly more expensive, are designed to last for the life of a printer. In some specialized material printers designed for laboratory research use, the printheads are of the piezoelectric type and made for a single-use.

In consumer-level printers, the most prevalent type of printhead is of the thermal variety. A thermal printhead is composed of an array of ink chambers formed by a photolithographic process and connected via supply lines to an ink supply. Each chamber has a resistive heating element that can rapidly vaporize an ink droplet. The vaporization of the ink droplet creates a bubble and the pressure difference across the bubble causes it to be ejected from the chamber and

onto paper. As it is being ejected, an additional supply of ink is drawn into the chamber in preparation for the next heating/jetting cycle.

Inks are colored with either dyes or pigments and must contain a volatile component in order for the bubble to form with heating. Controlling the heating elements in the ink chambers with a specific sequence of current flow prompts the jetting of the ink and allows for the formation of the desired print patterns on the target media.

A piezoelectric printhead, in contrast to thermal, does not use a heating element; ink is forced from chambers mechanically by charging a piezoelectric material. When charged, the piezoelectric element flexes, propelling the ink out through a nozzle. The lack of heat in the process eliminates the need for inks to have a volatile component, which allows for a wider range of materials to be printed. The material printing of titanium dioxide requires the use of piezoelectric printheads to prevent an aggregation of particles prior to deposition. Piezoelectric printheads are the primary type used in industrial and manufacturing applications. At the consumer level, Epson printers are made with fixed piezoelectric printheads that are designed to last for the life of the printer.

C.2.2 Suspension Requirements for Inkjet Printing

Three properties of a suspension determine whether it is printable: viscosity, surface tension, and maximum particle size. The viscosity—the measure of the fluid resistance to flow—of the suspension must be low enough for the printer to have sufficient driving force to move the solution through the feed system and for the spraying power of the piezoelectric printhead to be sufficient to jet a droplet. Too low a viscosity and the printer cannot control the jetting. The range of printable viscosities for an Epson printer has been determined as 1 cP to 20 cP, where cP is the centipoise unit [14]. Water at 20°C has a viscosity of 1cP. For the solution to not drip

out the printhead prior to jetting, the surface tension of the suspension must be high enough for it to be held in the nozzle. Surface tension cannot be too high else it will prevent printed droplets from spreading in the surface of the substrate. The range for this parameter has been found to be 28 mN/m^2 to 350 mN/m^2 [14].

The maximum particle size has to be limited to a value below the nozzle size in order to ensure that clogs do not develop. The size limit is determined by the ratio of the nozzle diameter to the volume distribution value of the suspension d_{v90}, the particle size that is greater than 90% of the particles present in the suspension. This ratio has been reported as 50:1 [8]. Solutions to the Naveir-Stokes equation can express these parameters as a single number known as the inverse Ohnesorge number, Z:

$$Z = \frac{(\alpha\rho\gamma)^4}{\eta} \qquad \text{(C-1).}$$

In equation C-1, α is the nozzle diameter, ρ is the suspension density, γ is the surface tension, and η is the viscosity. The range of Z for printable inks has been determined experimentally as $4<Z<14$ [8].

Appendix D: TiO_2 Suspension Stability

D.1 Aggregation

As Titanium dioxide (TiO_2) is not a soluble substance in any medium and because of the small masses, nanoparticles of TiO_2 have a natural tendency towards combining into clusters of one or more particles. Depending on the nature and strength of the particle bonding, these particles groupings are known either as aggregates or agglomerates[2]. Aggregates are strongly bonded particle clusters which are difficult to break apart without a directly applied force. Agglomerates, in contrast, are only loosely bonded particle groupings and can readily dissociate when certain properties of the solution are altered. TiO_2 particles readily form both aggregates and agglomerates when in aqueous solutions with a low or neutral ionic content.

Aggregates and agglomerates effectively function as individual particles of larger sizes leading to a decrease the overall surface area and fewer photo-sensitizer adsorption sites. Typical techniques used to reduce the presence of aggregates involve subjecting suspensions to attrition grinding, either through manual grinding effort in a mortar or by mechanically assisted means such as ball or planetary milling. Ultrasonic probes are also routinely used for the same purpose; the high frequency vibrations produced by the probe transfers mechanical energy for the disruption of the molecular forces holding the aggregates together.

In the context of DSSCs, an ideal TiO_2 mixture, in paste or suspension form, would contain no particle aggregations. Agglomerates can be normally be dissociated by adjustment of the suspension's ion concentration by the introduction to the suspension of highly acidic or highly basic chemicals.

[2] There is some inconsistency on this point in the literature: at times the terms are used interchangeably for any type of massed particle groupings, irrespective of whether they are weakly or tightly bonded.

The stability against aggregation of metal-oxide nanoparticles when dispersed in an aqueous media has become a topic of considerable interest over the past several years. Much of the interest has focused on developing stable suspension formulations to keep individual nanoparticles apart prior to delivery onto a target surface. When aggregation occurs, the favorably high surface area to volume ratio of the nanoparticles is diminished and specific delivery methods—such as dip-coating, screen-printing, or printing—may become inefficient or compromised resulting in non-uniform layers

Another motivation for an understanding of the suspension stabilities of nanoparticles relates to the particles' behavior when directly exposed to living cells. As one of the most commonly encountered nano-materials, TiO_2 has received significant scrutiny for potential adverse health effects. TiO_2 is one example of a metal-oxide material that has seen application in a large variety of commercial products covering a wide variety of uses. In bulk form, TiO_2 is considered to have a positive bio-compatibly.

When TiO_2 is reduced to or is generated in nano-particulate form, a new set of concerns arise, especially when the particles have the potential to be released into the environment. The concerns stem primarily from negative reactions to TiO_2 nanoparticles observed under laboratory conditions with exposed rats [26]. There is associated with these observations the belief that nanoparticles are able to penetrate living cells with ease and once inside, can proceed to disrupt cellular function, especially as individual particles aggregate into larger masses. Specific research questions being asked in this context relate to the range of naturally occurring conditions in which aggregation occurs as well as identifying measures that can serve to prevent that aggregation.

Investigations in this area have helped establish the range of conditions in which aggregation occurs and those in which it does not. One of the critical factors relating to the chance for aggregation is the pH of any aqueous environments into which the particles are released. A second factor is the presence and type of coating on the surface of the particles. Uncoated particles will, when in proximity with each other, aggregate with ease in an aqueous media with a neutral pH.

For a liquid to be pH neutral it must have an equal concentration of the two ions that form when water dissociates: hydrogen (H+), a positively charged ion, and hydroxide (-OH), a negative ion. The pH scale is logarithmic, runs from 1 to 14, and refers to the concentration of hydrogen ions. Pure water has an equal concentration of hydrogen and hydroxide ions and is defined as having a pH of 7. Below 7 on the pH scale, the solution will have a preponderance of hydrogen ions and is said to be acidic. Above 7 and the hydroxide ions dominate and the solution is referred to as basic.

D.2 Deposition Method-Specific Suspension Formulations

A number of methods are available for the deposition of nanoparticles. The principal objective of each is to produce a layer with a well-defined and consistent structure. A stable, uniform suspension ensures that an evenly deposited layer will have a consistent nano-structuring throughout once liquid components are driven off. The exact method for stabilizing the dispersion of the particles is determined by the requirements of the specific application. In electrophoretic deposition, for example, dispersing agents that bind directly to the nanoparticles are to be avoided as they interfere with attractive forces between surface charges and the opposite charges placed on a target surface [26].

As nanoparticles are insoluble, one option for achieving a stable suspension is to require that the aqueous media in which the particles are dispersed possess properties that counteract attractive intermolecular forces. This is primarily accomplished by modifying the pH in the surrounding bulk fluid [27]. A second approach to promote stability is to coat the particles with neutral or electrostatically repulsive materials [25]. The coating approach may be pursued in applications where the suspension must have a neutral pH or if the suspension requires a pH that falls within a range that does not promote dispersion stability. Such is the case for many inkjet printers which use a mildly basic ink pH to help prevent corrosion in the printing system but that requires extra precautions to prevent agglomeration of ink pigments.

D.3 Nanoparticle Electro-Chemistry

In a standard model of nanoparticle interactions, the Gouy-Chapman-Stern (GCS) model, a nanoparticle's surface charge will produce an electric field that attracts oppositely charged ions in the surrounding fluid medium [28]. The actual strength of the surface charge depends on the pH of the surrounding fluid and can equal zero if the pH is equal to the Isoelectric point (IEP) of the particles. The position of the IEP on the pH scale roughly determines the main pH regions of stability against aggregation.

When the field strength surrounding the particle has a large enough magnitude, a tightly packed layer of counter-ions, called the Stern layer, will form on the surface of the particle. If the surface charge on the particle is not fully screened by the Stern layer, additional ions are drawn in by Coulombic attraction. The secondary layer forms a diffuse arrangement of ions that extends from the particle surface to a distance equal to the Debye length. At the Debye length, the surface charge is sufficiently screened by ions to prevent additional ions from being securely held in place around the particle.

The electrostatic force generated by the surface charges present on the nanoparticle wall—the particle wall being the boundary between the solid material of the particle and the surrounding space—falls off exponentially. The Debye length for nanoparticles is often quite short in actual length but large in relation to the size of the nanoparticle. Taken together, the Stern and secondary ion layers are referred to as the Interfacial double layer or Electronic double layer (EDL). The interface between the double layer and the surrounding medium is called the Slipping plane [26]. The Slipping plane is the spatial limit of the nanoparticle to maintain a hold on ionic charges; inside the EDL the counter-ions are held with enough electrostatic force to ensure that they move in consert with the nanoparticle.

Figure C-1 provides a graphical representation of the GCS model with key elements identified.

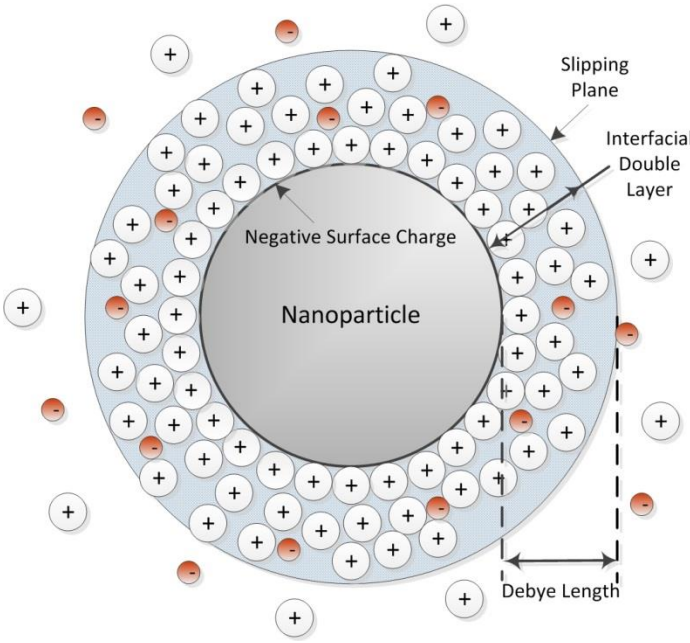

Figure C-1: A charged nanoparticle in suspension attracts oppositely charged ions to the surface, forming an interfacial double layer of ionic charges. The double layer extends out to the Debye length where surface charges are screened to a high enough degree to prevent a secure electrostatic hold on additional ions.

The potential of the Slipping plane interface is known as the zeta (ζ) potential. The ζ-potential, also referred to as the electrokinetic potential, is defined as the potential difference existing between the slipping plane of a particle's EDL and an arbitrarily defined neutral point within the surrounding bulk fluid [28]. According to the model, the inclination towards aggregation exhibited by dispersed nano-particles varies according to the ζ-potentials of the particles. A ζ-potential close to zero corresponds to a particle that does not carry enough repulsive force to prevent van der Waals forces and hydrogen bonding from leading to particle aggregation. Generally, a ζ-potential with a positive or negative magnitude greater than 40mV is sufficient to achieve moderate levels of suspension stability.

For TiO_2 nanoparticles, the value of the ζ-potential as a function of suspension pH has been well studied. The stable range of TiO_2 occurs for pH values which result in ζ-potentials of ±30mV. The precise boundaries of the stability range vary based on a number of factors including nanoparticle concentration, temperature, and the age of the suspension. The size and morphology of the nanoparticles will also influence the stability. Guiot and Spalla [26], based on a study of four different TiO_2 nanoparticles, identified a general range of dispersion instability for pH values between 5 and 9. Each of the TiO_2 particles studied by Guiot and Spalla were believed to have been coated with various substances to promote dispersion stability. Generally, ζ-potentials for TiO_2 have been found to be higher in magnitude for basic suspensions than for acidic ones. Lebrette et al. measured ζ-potentials greater in magnitude than -40mV for pH values greater than 7.5 and less than 2.5 [29]. TiO_2 powders with IEPs shifted to lower, acidic pH values have also been studied and show a corresponding shift down of the region of pH instability [25, 30].

D.4 Stabilizing Additives

A number of additives have been used in efforts to promote TiO_2 dispersion and control aggregation. Among the most common are alcohol based and include Poly ethylene glycol (PEG), glycerol, ethanol, and terpineol. The commonality in the chemical makeup of every alcohol is the presence of hydroxyl groups (-OH) bonded to carbon atoms. Two important characteristics of alcohol based additives, and why they are often preferred as stabilizing agents, is their chemical neutrality (pure alcohols have a pH of 7) and complete solubility in water. In applications where the suspension formulation requires a neutral, weakly acidic or weakly basic pH which would normally be in the unstable pH region, alcohols have been used to limit aggregation and promote dispersion. This also effectively simplifies the suspension processing in that pH adjustments to a particle's region of pH stability by addition of strong acids or bases may be unnecessary.

D.4.1 Poly Ethylene Glycol

Poly ethylene glycol (PEG) has seen broad usage in a variety of applications from food products to medicines. PEG is available in a number of molecular weights, from 200g/mol up to 20,000g/mol. Low molecular weight PEG has a highly viscous, waxy appearance and high molecular weights appear as solid crystalline flakes. All PEGs are readily soluble in a number of liquids including water, ethanol, and acetonitrile. The chemical structure of PEG molecules is $HO(CH_2CH_2O)_nH$ where the central portion is an ethylene unit repeated n times; the number of repeats determines the overall molecular weight of a particular PEG [31]. The usual practice is to refer to PEGs by molecular weight as opposed to the number of ethylene units in the chemical structure. Thus a PEG with 200g/mol weight is known as PEG200.

The process of coating a large molecule with PEG is known as PEGylation and prevents agglomeration by providing a non-ionic exterior shell that interferes with ionic bonding. Coating TiO_2 nanoparticles has also been demonstrated to significantly reduce the cytotoxicity associated with exposure of TiO_2 particles to living tissues [27].

The stability effect of PEGs of varied molecular weights when added to TiO_2 suspensions has been well studied. Kim and McKean observed that increasing the molecular weight of the PEG additive led to improvements in the stability of the suspensions against aggregation. Adding PEG20000 to TiO_2 suspensions was able to significantly reduce sedimentation when present in a 1:2 by weight ratio with TiO_2 powder [21]. To avoid an excess of free polymer in suspension, Kim and McKean suggested that a 1:2 ratio is too high based on a UV absorption spectrum obtained for prepared samples showing the presence of the polymers.

D.4.2 Ethanol

Alcohol-based chemicals, especially ethanol and terpineol, have a long history of usage as a primary solvent in DSSCs. For inkjet depositions of TiO_2 suspensions, water is often preferred for the main solvent to ethanol as it extends the drying time and helps prevent material buildup at the nozzles associated with rapid solvent evaporation. Still, a small addition of ethanol can help promote dispersion stability.

Lebrette et al. studied the effects of ethanol on the properties of TiO_2 suspensions [29]. A theoretical analysis suggests that the increase in ζ-potential is a consequence of a shift in the slipping plane further away from the particle surface. The surface charge of the particles and the ionic loading was not affected, however, suggesting that the ethanol was interfering with the hydrogen bond structure in the water, causing the shift in the slipping plane.

Appendix E: Equipment List

To complete the tasks required by the proposed objectives, additional materials, supplies, and equipment were procured, primarily for the milling apparatus. The entire material and equipment list, along with a description of each item's function in the project and approximate cost, is given in Table E-1. Chemicals and other items not listed in Table E-1 and that were used for solution preparations are detailed in the sections related to their use.

Table E-1: Material and equipment required for the research tasks, the quantity required, and the cost of the items procured specifically for the conducted research.

	Description	Quantity Needed	Cost (USD)
Inkjet Printer	Piezoelectric printhead-equipped printer with direct printing to substrate of custom suspensions	1	100
Ink Cartridges	Empty ink tanks; 1 required for each ink color of the printer	6	20 total
Syringes, needles, filters	Used to inject suspension into ink tanks	10	65 Total
Spin-Coater	High-speed spin-coater for the spin-on application of suspensions	1	NA
Conductive Glass Slides	Transparent conducting oxides; 2x2 inch slides were available and were cut to 4 1x1 inch slides	~80	Obtained from stock supply
TiO_2 nanoparticles	The material to be held dispersion in suspension for printing and spinning onto substrate	200 grams	Obtained from stock supply
PEG	Two molecular weights required, 600 and 20000 selected; used as dispersant, surfactant, and pore-forming agent	50 grams each	80 total
Denatured Alcohol	Solvent	500 ml	Obtained from stock supply
Milling Jar	Alumina milling jar with ceramic balls for attrition grinding of aggregates in suspension	1	160
Milling Carriage	Custom-made assembly to support milling jar while being rotated	1	20
Bench Grinder	Small, variable-speed grinder to drive the rotation of the milling jar	1	30

References

1. Hagfeldt, A., Boschloo, G., Sun, L., Kloo, L., & Pettersson, H. (2010). Dye-sensitized solar cells. *Chemical Review*, *110*, 6595-6663.

2. Jena, A., Mohanty, S. P., Kumar, P., Naduvath, J., Gondane, V., Lekha, P., Das, J., Narula, H. K., Mallick, S., & Phargava, P. (2012). Dye Sensitized Solar Cells: A review. *Transactions of Indian Ceramic Society, 71*(1), 1-16.

3. Wei, D., Andrew, P., & Ryhanen, T. (2010). Electrochemical photovoltaic cells - review of recent developments. *Journal of Chemical Technology and Biotechnology*, *85*, 1547-1552.

4. Mohammadi, M. R., Louca, R. R., Fray, D. J., & Welland, M. E. (2012). Dye-sensitized solar cells based on a single layer deposition of TiO2 from a new formulation paste and their photovoltaic performance. *Solar Energy*, *86*, 2654-2664.

5. Burschka, J., Pellet, N., Moon, S., Humphry-Baker, R., Gao, P., Nazeeruddin, M. K., & Gratzel, M. (2013). Sequential deposition as a route to high-performance perovskite-sensitized solar cells. *Nature*, *499*, 316-319. doi:10.1038/nature12340

6. Zhang, Q., & Cao, G. (2011). Nanostructured photoelectrodes for dye-sensitized solar cells. *Nano Today*, *2011*(9), 91-109.

7. Mohammadi, M. R., Louca, R. R., Fray, D. J., & Welland, M. E. (2012). Dye-sensitized solar cells based on a single layer deposition of TiO2 from a new formulation paste and their photovoltaic performance. *Solar Energy*, *86*, 2654-2664.

8. Kuscer, D., Stavber, G., Trefalt, G., & Kosec, M. (2012). Formulation of an aqueous titania suspension and its patterning with ink-jet printing technology. *Journal of The American Ceramic Society, 95*(2), 487-493.

9. Cerna, M., Vesely, M., & Dzik, P. (2011). Physical and chemical properties of titanium dioxide printed layers. *Catalysis Today, 161*, 97-104.

10. Wang, Z, Kawauchi, H, Kashima, T, Arakawa, H, (2004). Significant influence of TiO2 photoelectrode morphology on the energy conversion efficiency of N719 dye-sensitized solar cell. *Coordination Chemistry Reviews*, 248, Issues 13–14, 1381-1389.

11. Morozova, M., Kluson, P., Krysa, J., Vesely, M., Dzik, P., & Solcova, O. (2012). Electrochemical properties of TiO2 electrode prepared by various methods. *Procedia Engineering*, *42*, 573-580.

12. Ito, S., Chem, P., Comte, P., Nazeeruddin, M. K., Liska, P., Pechy, P., & Gratzel, M. (2007). Fabrication of screen-printing pastes from TiO2 powders for dye-sensitised solar cells. *Prog. Photovolt: Res. Appl*, *15*(7), 603-612.

13. Jourdani, R., Outzourhit, A., Oueriagli, A., Aitelhabti, D., Ameziane, E. L., Barazzouk, S., & Hotchandani, S. (2004). Structural, optical and electrochromic properties of nanocrystalline TiO2 thin films prepared by spin coating. *Active and Passive Electronic Components*, *27*, 125-131.

14. Yang, M., Li, L., Zhang, S., Li, G., & Zhao, H. (2010). Preparation, characterization and sensing application of inkjet-printed nanostructured TiO2 photoanode. *Sensors and Actuators B: Chemical*, *147*, 622-628.

15. Fan, K., Liu, M., Peng, T., Ma, L., & Dai, K. (2010). Effects of paste components on the properties of screen-printed porous TiO2 film for dye-sensitized solar cells. *Renewable Energy*, *35*, 555-561.

16. Dang, M. C., Dang, T. M., & Fribourg-Blanc, E. (2013). Inkjet printing technology and conductive inks synthesis for microfabrication techniques. *Advances in Natural Sciences: Nanoscience and Nanotechnology*, *4*(1), 1-7.

17. Su, C., Hung, W., Lin, C., & Chien, S. (2010). The preparation of composite TiO2 electrodes for dye-sensitized solar cells. *Journal of the Chinese Chemical Society*, *57*, 1131-1135.

18. Lejeune, M., Chartier, T., Dossou-Yovo, C., & Noguera, R. (2009). Inkjet printing of ceramic micro-pillar arrays. *Journal of the European Ceramic Society*, *29*, 905-911.

19. Arin, M., Lommens, P., Avci, N., Hopkins, S. C., De Buysser, K., Arabatzis, I. M., Fasaki, I., Poelman, D., & Van Driessche, I. (2011). Inkjet printing of photocatalytically active TiO2 thin films from water based precursor solutions. *Journal of the European Ceramic Society*, *31*, 1067-1074.

20. Morozova, M., Kluson, P., Krysa, J., Dzik, P., Vesely, M., & Solcova, O. (2011). Thin TiO2 films prepared by inkjet printing of the reverse micelles sol-gel composition. *Sensors and Actuators B: Chemical*, *160*, 371-378.

21. Kim, S., & McKean, D. (1998). Aqueous TiO2 suspension preparation and novel application of ink-jet printing technique for ceramics patterning. *Journal of Materials Science Letters*, *17*, 141-144.

22. Oh, Y., Yoon, H. G., Lee, S., Kim, H., & Kim, J. (2012). Inkjet-printing of TiO2 co-solvent ink: From uniform ink-droplet to TiO2 photoelectrode for dye-sensitized solar cells. *Journal of the Electrochemical Society*, *159*(1), 35-39.

23. Epson.com (2013, September). *PrecisionCore White Paper*. Retrieved October 15, 2013, from

http://www.epson.com/_alfresco/LandingPages/landing/PrecisionCore/PrecisionCore_White_Paper.pdf

24. Chovancova, V., Howell, P., Fleming III, P. D., & Rasmusson, A. (2004). Printability of different Epson ink jet ink sets. *Proc. IS&T?s 20th International Conference on Digital Printing Technologies*, 457-463. Retrieved from https://www.wmich.edu/pci/faculty/Publication/fleming/NIP-20-98.pdf

25. Mano, S. S., Kanehira, K., Sonezaki, S., & Taniguchi, A. (2012). Effect of Polyethylene Glycol Modification of TiO_2 Nanoparticles on Cytotoxicity and Gene Expressions in Human Cell Lines. *Internation Journal of Molecular Sciences*, *13*(3), 3703-3717. doi:10.3390/ijms13033703

26. Hanaor, D., Michelazzi, M., Veronesi, P., Leonelli, C., Romagnoli, M., & Sorrell, C. (2011). Anodic aqueous electrophoretic deposition of titanium dioxide using carboxylic acids as dispersing agents. *Journal of the European Ceramic Society*, *31*, 1041-1047. doi:10.1016/j.eurceramsoc.2010.12017

27. Guiot, C., & Spalla, O. (2012). Stabilization of TiO_2 nanoparticles in complex medium through pH adjustment protocol. *Environmental Science and Technology*, *47*(2), 1057-1064. doi:10.1021/es3040736

28. Kirby, B. J. (2010). *Micro- and Nanoscale Fluid Mechanics: Transport in Microfluidic Devices*. New York, NY: Cambridge University Press.

29. Lebrette, S., Pagnoux, C., & Abélard, P. (2004). Stability of aqueous TiO_2 suspensions: influence of ethanol. *Journal of Colloid and Interface Science*, *280*(2), 400-408.

30. Sentein, C., Guizard, B., Giraud, S., Ye, C., & Tenegal, F. (2009). Dispersion and stability of TiO_2 nanoparticles synthesized by lase pyrolysis in aqueous suspensions. *Journal of Physics: Conference Series, 170*(1), 1-7. doi:10.1088/1742-6596/170/1/012013

31. CHEMINDUSTRY.RU (n.d.). *Polyethylene glycol: chemical product information at CHEMINDUSTRY.RU*. Retrieved October 15, 2013, from http://chemindustry.ru/Polyethylene_Glycol.php

32. Goncalves, L. M., De Zea Bermudez, V., Ribeiro, H. A., & Mendes, A. M. (2008). Dye-Sensitized solar cells: A safe bet for the future. *Energy and Environmental Science*, *1*, 655-667.

33. Zhang, Q., & Cao, G. (2011). Nanostructured photoelectrodes for dye-sensitized solar cells. *Nano Today, 2011*(9), 91-109.

34. Mehta, S. (2011, May 9). *PV News Annual Data Collection Results: 2010 Cell, Module Production Explodes Past 20 GW : Greentech Media*. Retrieved from http://www.greentechmedia.com/articles/read/pv-news-annual-data-collection-results-cell-and-module-production-explode-p/

35. Choubey, P. C., Oudhia, A., & Dewangan, R. (2012). A review: Solar cells current scenario and future trends. *Recent Research in Science and Technology*, *4*(8), 99-101.

36. Nelson, J. (2003). *The Physics of Solar Cells*. Imperial College Press.

37. Ito, S., Ha, N., Rothenberger, G., Liska, P., Comte, P., Zakeeruddin, S. M., Pechy, P., Nazeeruddin, M. K., & Gratzel, M. (2006). High-efficiency (7.2%) flexible dye-sensitized solar cells with Ti-metal substrate for nanocrystalline-TiO2 photoanode. *Chem. Commun*, *2006*, 4004-4006.

38. Marti, A., & Araujo, G. (1996). Limiting efficiencies for photovoltaic energy conversion in multigap systems. *Solar Energy Materials and Solar Cells*, *43*(2), 203-222.

39. Jena, A., Mohanty, S. P., Kumar, P., Naduvath, J., Gondane, V., Lekha, P., Das, J., Narula, H. K., Mallick, S., & Phargava, P. (2012). Dye Sensitized Solar Cells: A review. *Transactions of Indian Ceramic Society*, *71*(1), 1-16.

40. Jasim, K. E. (2011). Dye sensitized solar cells - Working principles, challenges and opportunities. In L. A. Kosyachenko (Ed.), *Solar Cells - Dye-Sensitized Devices* (pp. 171-204). InTech.

41. Schiffmann, F., VandeVondele, J., Hutter, J., Urakawa, A., Wirz, R., & Baiker, A. (2010). An atomistic picture of the regeneration process in dye sensitized solar cells. *PNAS*, *107*(11), 4830-4833.

42. Bowers, J. W., Upadhyaya, H. M., Calnan, S., Hashimoto, R., Nakada, T., & Tiwari, A. N. (2009). Development of nano-TiO2 dye sensitized solar cells on high mobility transparent conducting oxide thin films. *Progress in Photovoltaics: Research and Applications*, *17*, 265-272.

43. Ma, T., Fang, X., Akiyama, M., Inoue, K., Noma, H., & Abe, E. (2004). Properties of several types of novel counter electrodes for dye-sensitized solar cells. *Journal of Electroanalytical Chemistry*, *574*, 77-83.

44. Murakami, T., & Gratzel, M. (2007). Counter electrodes for DSC: Application of functional materials as catalysts. *Inorganica Chimica Acta*, *361*(2008), 572-580.

45. Ren, D., Zou, Y., Zhan, C., & Huang, N. (2010). Behaviors of different dispersers on morphologies of porous TiO2 films. *Front. Mater. Sci. China*, *4*(4), 394-397.

46. Bang, H., Chung, J., Jung, R., & Park, S. (2012). Effect of acetic acid in TiO2 paste on the performance of dye-sensitized solar cells. *Ceramics International*, *38*, 511-515.

47. Narayan, M. R. (2012). Review: Dye sensitized solar cells based on natural photosensitizers. *Renewable and Sustainable Energy Reviews*, *16*(2012), 208-215.

48. Jasim, K. E. (2012). Natural dye-sensitized solar cell based on nanocrystalline TiO2. *Sains Malaysiana*, *41*(8), 1011-1016.

49. McGehee, M. D. (2011). Paradiam Shifts in dye-sensitized solar cells. *Science*, *334*, 607-608.

50. Harikisun, R., & Desilvestro, H. (2011). Long-term stability of dye solar cell. *Solar Energy*, *85*, 1179-1188.

51. Li, D., Qin, D., Deng, M., Lou, Y., & Meng, Q. (2008). Optimization of the solid-state electrolytes for dye-sensitized solar cells. *Energy and Environmental Science*, *2*, 283-291.

52. Yum, J., Chen, P., Gratzel, M., & Nazeeruddin, M. K. (2008). Recent developments in solid-state dye-sensitized solar cells. *ChemSusChem*, *1*, 699-707.

53. Bailey, S. G., Castro, S. L., Raffaelle, R. P., Fahey, S., Gennett, T., & Tin, P. (2003). Nanostructured materials for solar cells. *3rd World Conference on Photovoltaic Energy Conversion*, 2690-2693.

54. Kamat, P. V. (2012). Boosting the efficiency of quantum dot sensitized solar cells through modulation of interfacial charge transfer. *Accounts of Chemical Research*, *45*(11), 1906-1915.

55. Zhang, Y., Huang, X., Gao, K., Yang, Y., Lou, Y., Li, D., & Meng, Q. (2011). How to design dye-sensitized solar cell modules. *Solar Energy Materials & Solar Cells*, *95*, 2564-2569.

56. Wang, L., Fang, X., & Zhang, Z. (2010). Design methods for large scale dye-sensitized solar modules and the progress of stability research. *Renewable and Sustainable Energy Review*, *14*, 3178-3184.

57. Leonardi, E., Penna, S., Brown, T. M., Carlo, A. D., & Reale, A. (2010). Stability of dye-sensitized solar cells under light soaking test. *Journal of Non-Crystalline Solids*, *358*, 2049-2052.

58. Kato, N., Higuchi, K., Tanaka, H., Nakajima, J., Sano, T., & Toyoda, T. (2011). Improvement in long-term stability of dye-sensitized solar cell for outdoor use. *Solar Energy Materials & Solar Cells*, *95*, 301-305.

59. Likodimos, V., Stergiopoulos, T., Falaras, P., Harikisun, R., Desilvestro, J., & Tulloch, G. (2009). Prolonged light and thermal stress effects on industrial dye-sensitized solar cells: A micro-Raman investigation on the long-term stability of aged cells. *J. Phys. Chem*, *113*, 9412-9422.

60. Chen, X., & Mao, S. S. (2007). Titanium dioxide nanomaterials: Synthesis, properties, modifications, and applications. *Chemical Reviews*, *107*(7), 2891-2959.